

AD-A118 591

SOUTH CAROLINA UNIV COLUMBIA COLL OF ENGINEERING

F/6 20/4

UNSTEADY BOUNDARY LAYER DUE TO AN OSCILLATING FREE STREAM VS. A--ETC(U)

JUN 82 D E WILSON

AFOSR-80-0182

UNCLASSIFIED

AFOSR-TR-82-0675

NL

1 OF 1

AD-A118 591

END

DATE

FILED

09-82

DTIC

AFOSR-TR- 82 - 0675

13

AD A118591

UNSTEADY BOUNDARY LAYER DUE
TO AN OSCILLATING FREE STREAM
VS. AN OSCILLATING MODEL

FINAL AFOSR REPORT
80-00936
June 25, 1982

AFOSR-80-0182

DTIC
ELECTE
AUG 25 1982
S D H

DTIC FILE COPY

Approved for public release;
distribution unlimited.

82 08 25 001

REPORT DOCUMENTATION PAGE		READ INSTRUCTIONS BEFORE COMPLETING FORM
1. REPORT NUMBER AFOSR-TR- 82 - 0675	2. GOVT ACCESSION NO. AD-A118591	3. RECIPIENT'S CATALOG NUMBER
4. TITLE (and Subtitle) UNSTEADY BOUNDARY LAYER DUE TO AN OSCILLATING FREE STREAM VS AN OSCILLATING MODEL		5. TYPE OF REPORT & PERIOD COVERED FINAL 15 May 80 - 14 May 81
		6. PERFORMING ORG. REPORT NUMBER
7. AUTHOR(s) DENNIS E WILSON		8. CONTRACT OR GRANT NUMBER(s) AFOSR-80-0182
9. PERFORMING ORGANIZATION NAME AND ADDRESS UNIVERSITY OF SOUTH CAROLINA COLLEGE OF ENGINEERING COLUMBIA, SC 29208		10. PROGRAM ELEMENT, PROJECT, TASK AREA & WORK UNIT NUMBERS 61102F 2307/D9
11. CONTROLLING OFFICE NAME AND ADDRESS AIR FORCE OFFICE OF SCIENTIFIC RESEARCH/NA BOLLING AFB, DC 20332		12. REPORT DATE 25 June 1982
		13. NUMBER OF PAGES 56
14. MONITORING AGENCY NAME & ADDRESS (if different from Controlling Office)		15. SECURITY CLASS. (of this report) Unclassified
		15a. DECLASSIFICATION/DOWNGRADING SCHEDULE
16. DISTRIBUTION STATEMENT (of this Report) Approved for Public Release; Distribution Unlimited.		
17. DISTRIBUTION STATEMENT (of the abstract entered in Block 20, if different from Report)		
18. SUPPLEMENTARY NOTES		
19. KEY WORDS (Continue on reverse side if necessary and identify by block number) UNSTEADY BOUNDARY LAYER OSCILLATING FLOW UNSTEADY VISCOUS - INVISCID INTERACTION		
20. ABSTRACT (Continue on reverse side if necessary and identify by block number) The objective of this investigation is to calculate the unsteady boundary layer induced on a thin airfoil by two distinct mechanisms. First, a uniform upstream flow approaches an airfoil which is undergoing a periodic transverse oscillation of specified frequency and amplitude with respect to the wind tunnel. And secondly, a uniform upstream flow approaches the same airfoil which is fixed with respect to the wind tunnel but is now subjected to transverse oscillating flow. The transverse flow is produced at the walls of the wind tunnel test section and will contain a spatial distribution at the test section centerline.		

UNCLASSIFIED

SECURITY CLASSIFICATION OF THIS PAGE(When Data Entered)

The method employed in this analysis uses the classical potential flow/boundary layer interaction. The mathematical model assumes a laminar incompressible flow over a two-dimensional thin airfoil. In addition, the amplitude of the transverse oscillation is assumed to be small with respect to the chord of the airfoil. This restriction is also equivalent to small transverse velocities relative to the upstream flow, if the frequencies are moderate. This assumption produces a set of linear disturbance equations for the unsteady flow. No other restrictions are placed upon the spatial distribution of the transverse flow, although results are presented only for cosine distribution which represents the worst possible case.

UNCLASSIFIED

SECURITY CLASSIFICATION OF THIS PAGE(When Data Entered)

TABLE OF CONTENTS

	Page
1.0 INTRODUCTION	2
2.1 MATHEMATICAL FORMULATION	7
2.1 Potential Flow Formulation	8
2.2 Boundary Layer Formulation	9
2.3 Nondimensional and Perturbation Equations	9
3.0 POTENTIAL FLOW SOLUTION	15
3.1 Thin Airfoil Solution	15
3.1.1 Vertical Oscillation of Airfoil	17
3.1.2 Vertical Oscillation of Free Stream	18
3.2 Leading Edge Solution	20
4.0 BOUNDARY LAYER RESULTS	23
4.1 Thin Airfoil Solution	23
4.2 Leading Edge Solution	26
4.3 Results and Discussion	28
5.0 APPENDIXES	32
6.0 REFERENCES	47
7.0 FIGURES	48

Accession For	
NTIS GRA&I	<input checked="" type="checkbox"/>
DTIC TAB	<input type="checkbox"/>
Unannounced	<input type="checkbox"/>
Justification	
By	
Distribution/	
Availability Codes	
Dist	Avail and/or
	Special
A	



AIR FORCE OFFICE OF SCIENTIFIC RESEARCH (AFSC)
 NOTICE OF TRANSMITTAL TO DTIC
 This technical report has been reviewed and is
 approved for transmittal to DTIC APR 199-12.
 Distribution is unlimited.
 MATTHEW J. MILLER
 Chief, Technical Information Division

1.0 INTRODUCTION

A considerable amount of theoretical and numerical analysis has been published recently in the general area of unsteady flows and, in particular, on unsteady transonic flows. However, at the same time there is a shortage of experimental results [1]. The capabilities of ground test facilities have actually been surpassed by analytical and computational methods in many areas of unsteady aerodynamics. One reason is the inherent problem of obtaining detailed measurements about a moving model. However, a large class of unsteady flow experiments can be conducted with stationary models when a controlled oscillatory flow is generated in the test section. These so called gust tunnels have demonstrated the potential of providing valuable aerodynamic data [2].

Unfortunately, with few exceptions [3], all existing gust tunnels are small, low speed facilities. Recently, however, a new concept termed the "Ball Wall" has been used to introduce oscillations in the transverse velocity over a wide range of speeds [4]. The new concept utilizes a temporal variation of the test section wall porosity to produce a frequency range of flow perturbations within the test section that is unique relative to other gust tunnels. Measureable flow angularity oscillations were generated at frequencies from quasi-steady to 50 Hz in tunnel (4T) at the Arnold Engineering Development Center [4].

Having demonstrated the experimental capability of producing a controlled oscillatory flow from subsonic incompressible to the transonic flow regime, a serious question arose concerning the dynamic similarity due to an oscillating flow as opposed to an oscillating model of equal frequency and amplitude. Specifically, the question is: is the velocity

distribution in the neighborhood of the model and the resulting normal and shear stress distribution equivalent when the free stream contains a periodic transverse oscillation which is equal in magnitude to transverse model oscillation?

It is well known [5] that for compressible flow the two problems of fixed bodies in oscillating flows and oscillation bodies in steady uniform flows are not equivalent. The discrepancy is due to the inertia term introduced in the boundary layer equations when transforming from the fixed to the oscillating coordinate system. Thus, the boundary layer equations are different, and as expected the near field velocity distribution is not equivalent for the two cases.

A common misconception is that for incompressible flows the two problems are always equivalent, although for certain in-plane oscillations equivalent surface stress distributions are produced. One example of equivalent transverse oscillations is the two-dimensional stagnation point flow generated by an infinite flat plate. A uniform flow, U_∞ , approaching a plane wall which oscillates with velocity, V_p , given by $V_p = V_0 \cos \omega t$ produces the equivalent wall shear stress distribution as that of a fixed wall which sees a uniform flow with an equivalent transverse component which is π out of phase. These two problems were first investigated by Glauert [6] and the kinematic and geometric similarity which produces the equivalent dynamic effects is physically obvious. In fact a simple coordinate transformation from one fixed in space to one fixed to the stagnation point demonstrates the equivalence [6].

Now consider the two distinct problems of a right circular cylinder undergoing small transverse oscillations in a steady uniform flow and what appears to be the similar problem of a stationary cylinder subjected to a

steady uniform flow which contains the equivalent transverse oscillations, i.e. equal frequency and magnitude. For the idealized situation all points in the flow field have the same vertical oscillation, which is different from the so-called gust problem where a periodic component is convected down stream. The gust condition may be a more realistic model for the conditions created in some wind tunnels, however it is obvious that the flow field for this condition is not even kinematically similar to the case of an oscillating cylinder.

If the potential flow field due to a steady uniform form, U_∞ , plus a small transverse oscillating component, given by $V_0 \cos \omega t$ is solved, the resulting surface velocity for an (r, θ) coordinate system fixed to the cylinder is

$$V_\theta(R, \theta, t) = -2U_\infty \sin \theta - 2V_0 \cos \omega t \cos \theta.$$

The stagnation point is then displaced through maximum angle given by $\tan \phi_{S.P.} = \frac{V_0}{U_\infty}$.

Now consider the corresponding potential flow problem of a uniform steady flow approaching a cylinder undergoing a vertical oscillation of identical frequency and amplitude but with a 180° phase difference. Solving this problem by an analysis similar to that of G. I. Taylor [7], the resulting surface velocity is given by

$$v_\theta(R, \theta, t) = 2U_\infty \sin \theta - V_0 \cos \omega t \cos \theta.$$

It is seen that the unsteady part of $v_\theta(R, \theta, t)$ is different and in fact the maximum stagnation point excursion is exactly one-half that of the first case. It then follows that the surface shear stress distribution will also be different, and in the linearized case of small transverse

oscillations is one-half that of the first case. The reason for the factor of two discrepancy is due to the physical difference in the two flow fields. In the first problem, the entire flow field oscillates in time and the presence of the cylinder is essentially ignored. There is no circulation and the flow is symmetric about the dividing streamline, a condition which closely approximates the quasi-steady viscous problem. In the second case the flow field is basically steady, and the unsteady effects are limited to a small region around the cylinder, known as the added mass region. An observer fixed on the cylinder sees a negative velocity, V_0 , at infinity, however as the particles approach the cylinder, they experience a slowly increasing positive velocity field. The net effect is to produce an asymmetric flow and a stagnation point deflection of one-half that of the first case.

From this example, even when all points in the flow field contain a spatially uniform and instantaneously oscillating transverse component, it is seen that there is a difference in the near field fluid mechanics. The differences can become more pronounced, when in fact the spatial distribution is not quite uniform. This is in fact what occurs near the beginning of the porous wall region, especially when the freestream velocity is large [4] and the length of the porous wall is of the same order as the model.

Having gained some physical insight into the subtle differences of the two unsteady problems, i.e. oscillation flow fields vs. oscillating bodies, during the AFOSR Summer Research Program, it was decided to study the unsteady fluid dynamics around a restricted class of airfoils. Specifically, the investigation is limited to airfoils having small thick-

ness ratios so that thin airfoil theory can be employed. This leads to considerable simplifications in the unsteady potential flow analysis and the subsequent numerical integration of the boundary layer equations.

2.0 MATHEMATICAL FORMULATION

The basic problem considered in this investigation is an unsteady laminar incompressible flow over a two-dimensional thin airfoil. The concept of a thin airfoil as used in this analysis implies that $t/b \ll 1$ as shown in Figure 1. This implies that the mean chord of the airfoil lies along the X axis to within $O[\epsilon]$, where $\epsilon \equiv a/b$ and $a/t = O[1]$. This implies that disturbances to the free stream flow generated by the airfoil are $O[\epsilon]$. This formulation has distinct mathematical advantages which will be explored in the following analysis. First, it allows for an analytical solution to the potential flow field to within $O[\epsilon^2]$. And secondly, it permits a very accurate and stable hybrid numerical scheme to be employed for the solution of the boundary layer equations. Although the thin airfoil approximation limits the physical application of the analysis, its simplicity allows for both physical insight into the unsteady effects, and provides a valuable base line analysis for comparison to subsequent studies which can include airfoil thickness, camber, and angle of attack.

Specifically, the purpose of this analysis is to compare the effects of two distinct unsteady flows under the thin airfoil approximation. First, a uniform free stream approaches the airfoil which is undergoing a periodic transverse oscillation with respect to the x-y axis of amplitude a and frequency ω as shown in Figure 2a. And secondly, a uniform flow plus a periodic transverse component approach the same airfoil which is now fixed with respect to the X-Y axis. This part of the analysis is sufficiently general so that any spatial distribution in the transverse component capable of being represented by a Fourier series can be consider-

ed. For both conditions the amplitude of the oscillation is "small", i.e., $a/b \ll 1$. This implies that both the airfoil geometry and the unsteady effect will appear first in the $O[\epsilon]$ equations.

2.1 Potential Flow Formulation

In addition to the previous restrictions, the fluid will be assumed inviscid in this section. This is reasonable under thin airfoil theory, since without separation the viscous effects are confined to the boundary layer and the effect of viscosity can be incorporated by a phenomenological rule that the velocity at the trailing edge must remain finite and tangent to the airfoil surface. Finally, in addition to the inviscid assumption, the fluid will be taken as piezotropic, i.e., $\rho = \rho(p)$ only.

The equations will be formulated in terms of the acceleration potential, ϕ , of the flow field. This approach is selected because ϕ is continuous throughout the idealized wake in thin airfoil theory whereas the usual velocity potential is discontinuous. A detailed discussion of the derivation of the equations can be found in Ref. [8]. In this section, we simply note that the relevant equations are Euler's equation written as

$$\frac{D\vec{V}}{Dt} = - \nabla \int_{p_0}^p \frac{dp}{\rho} \quad , \quad (1)$$

and, the acceleration potential definition is given by

$$\nabla \phi = \frac{D\vec{V}}{Dt} \quad (2)$$

Substituting equation (2) into (1) and integrating with respect to space yields

$$\phi + \int_{P_0}^P \frac{dP}{\rho} = \text{constant} \quad (3)$$

Further simplifications plus a discussion of the boundary conditions will be made in Section 2.3.

2.2. Boundary Layer Formulation

The two dimensional, incompressible, unsteady, laminar boundary layer equations in terms of the stream function are

$$\frac{\partial^2 \psi}{\partial t \partial y} + \frac{\partial \psi}{\partial y} \frac{\partial^2 \psi}{\partial x \partial y} - \frac{\partial \psi}{\partial x} \frac{\partial^2 \psi}{\partial y^2} = - \frac{1}{\rho} \frac{\partial p}{\partial x} + \nu \frac{\partial^3 \psi}{\partial y^3} \quad (4)$$

where $u \equiv \frac{\partial \psi}{\partial y}$ and $v \equiv - \frac{\partial \psi}{\partial x}$.

The unsteady pressure gradient is given by

$$- \frac{1}{\rho} \frac{\partial p}{\partial x} = \frac{\partial U_e}{\partial t} + U_e \frac{\partial U_e}{\partial x} \quad (5)$$

Adopting the usual body coordinate system shown in Figure 3, the boundary conditions become

$$\frac{\partial \psi}{\partial y} = \frac{\partial \psi}{\partial x} = 0 \quad \text{at } y = 0 \quad (6a,b)$$

and

$$\frac{\partial \psi}{\partial y} \rightarrow U_e(x,t) \quad \text{as } y \rightarrow \infty \quad (6c)$$

In equation (6c), $U_e(x,t)$ represents the velocity at the edge of the boundary layer which will be determined from the potential flow solution.

2.3. Nondimensionalization and Perturbation Equations

Outside the leading edge region, two important length scales

characterize the unsteady boundary layer. They are δ_S and δ_B , where $\delta_S \sim (\nu/\omega)^{1/2}$ and $\delta_B \sim (\nu x/U_\infty)^{1/2}$. If no steady flow is present, the fluctuating part of the flow extends a distance δ_S away from the surface. When a steady flow is superimposed, the two layers interact and the resulting flow can be quite complicated when the two layers are of comparable magnitude, i.e. $\frac{\omega x}{U_\infty} = O[1]$. However, under certain restrictions the mathematical analysis can be dramatically simplified. This occurs if we restrict the magnitude of the transverse oscillating component, V_0 , such that $V_0/U_\infty \ll 1$. This does not limit the analysis since, by definition of the problem, V_0 is less than about 10% of the free stream velocity due to physical limitations of the wind tunnel. Referring to Figure 2, we see that $V_0 \sim \omega a$, thus $\omega a/U_\infty \ll 1$. This can be written as $(\omega b/U_\infty)\epsilon \ll 1$, where $\epsilon \equiv a/b$. This implies $\omega b/U_\infty = O[1]$ or equivalently $\omega x/U_\infty = O[1]$ except near the leading edge of the airfoil. However by definition, the boundary layer analysis excludes this region, thus we conclude $\omega x/U_\infty = O[1]$.

The parameter $\frac{\omega b}{U_\infty}$ has a special significant, consequently we let $\alpha \equiv 2b\omega/U_\infty$, and $\alpha = O[1]$ implies that the two layers are of comparable magnitude, and either δ_S or δ_B are acceptable length scales. However, since $\epsilon \rightarrow 0$ implies the oscillatory component vanishes, δ_B is more appropriate. Accordingly the following nondimensional variables and parameters are selected for the boundary layer phase of the analysis.

$$\eta \equiv \frac{y}{(\frac{2b\nu}{U_\infty})^{1/2}}, \quad \zeta \equiv \frac{x}{2b}, \quad \tau \equiv \omega t$$

$$\bar{P} \equiv \frac{P}{\rho U_\infty^2}, \quad \bar{U} \equiv \frac{U}{U_\infty}, \quad \bar{V} \equiv \frac{V}{U_\infty} Re^{1/2} \quad (7)$$

$$R_e \equiv \frac{2bU_\infty}{\nu}, \quad \bar{\psi} \equiv \frac{\psi}{(2b\nu U_\infty)^{1/2}}, \quad \alpha \equiv \frac{2b\omega}{U_\infty}, \quad \epsilon \equiv \frac{a}{b}, \quad (7)$$

Substituting equations (7) into equation (4) yields

$$\alpha \frac{\partial^2 \bar{\psi}}{\partial \tau \partial \eta} + \frac{\partial \bar{\psi}}{\partial \eta} \frac{\partial^2 \bar{\psi}}{\partial \zeta \partial \eta} - \frac{\partial \bar{\psi}}{\partial \zeta} \frac{\partial^2 \bar{\psi}}{\partial \eta^2} - \frac{\partial^3 \bar{\psi}}{\partial \eta^3} = - \frac{\partial \bar{p}}{\partial \zeta} \quad (8)$$

where

$$- \frac{\partial \bar{p}}{\partial \zeta} = \alpha \frac{\partial \bar{U}_e}{\partial \tau} + U_e \frac{\partial \bar{U}_e}{\partial \zeta} \quad (9)$$

with the following boundary conditions.

$$\frac{\partial \bar{\psi}}{\partial \eta} = \frac{\partial \bar{\psi}}{\partial \zeta} = 0 \quad \text{at} \quad \eta = 0 \quad (10a,b)$$

$$\frac{\partial \bar{\psi}}{\partial \eta} \rightarrow \bar{U}_e \quad \text{as} \quad \eta \rightarrow \infty \quad (10c)$$

From the physical description of the problem, it is reasonable to expect that both the edge velocity, U_e , and the pressure gradient calculated from potential flow theory can be expressed as

$$\bar{U}_e(\zeta, \tau) = \bar{U}_0 + \epsilon \bar{U}_1(\zeta, \tau) + O[\epsilon^2] \quad (11)$$

and

$$\bar{P}(\zeta, \tau) = \bar{P}_0 + \epsilon \bar{P}_1(\zeta, \tau) + O[\epsilon^2] \quad (12)$$

It then follows that the stream function can be written as

$$\bar{\psi}(\zeta, \eta, \tau; \alpha, \epsilon) = \bar{\psi}_0(\zeta, \eta; \alpha) + \epsilon \bar{\psi}_1(\zeta, \eta, \tau; \alpha) + O[\epsilon^2] \quad (13)$$

Substituting equation (13) into the stream function equation yields the following two equations.

$$\frac{\partial \bar{\psi}_0}{\partial \eta} \frac{\partial^2 \bar{\psi}_0}{\partial \zeta \partial \eta} - \frac{\partial \bar{\psi}_0}{\partial \zeta} \frac{\partial^2 \bar{\psi}_0}{\partial \eta^2} - \frac{\partial^3 \bar{\psi}_0}{\partial \eta^3} = - \frac{\partial \bar{p}_0}{\partial \zeta} \quad (14)$$

and

$$\alpha \frac{\partial^2 \bar{\psi}_1}{\partial \tau \partial \eta} + \bar{\psi}_{0,\eta} \frac{\partial^2 \bar{\psi}_1}{\partial \zeta \partial \eta} + \bar{\psi}_{0,\zeta \eta} \frac{\partial \bar{\psi}_1}{\partial \eta} - \bar{\psi}_{0,\zeta} \frac{\partial^2 \bar{\psi}_1}{\partial \eta^2} - \bar{\psi}_{0,\eta \eta} \frac{\partial \bar{\psi}_1}{\partial \zeta} - \frac{\partial^3 \bar{\psi}_1}{\partial \eta^3} = - \frac{\partial \bar{p}_1}{\partial \zeta} \quad (15)$$

In equation (15) the notation $\bar{\psi}_{0,\eta} \equiv \partial \bar{\psi}_0 / \partial \eta$ is adopted for simplicity.

The corresponding set of boundary conditions become

$$\frac{\partial \bar{\psi}_0}{\partial \eta} = \frac{\partial \bar{\psi}_0}{\partial \eta} = 0 \quad \text{at } \eta = 0 \quad (16a,b)$$

$$\frac{\partial \bar{\psi}_0}{\partial \eta} \rightarrow \bar{U}_0 \quad \text{as } \eta \rightarrow \infty \quad (16c)$$

and

$$\frac{\partial \bar{\psi}_1}{\partial \eta} = \frac{\partial \bar{\psi}_1}{\partial \zeta} = 0 \quad \text{at } \eta = 0 \quad (17a,b)$$

$$\frac{\partial \bar{\psi}_1}{\partial \eta} \rightarrow \bar{U}_1 \quad \text{as } \eta \rightarrow \infty \quad (17c)$$

In the potential flow region, the characteristic length scale for both X and Y is simply one-half the airfoil chord, b . The velocity scale is the free stream velocity, U_∞ . The time and acceleration potential are nondimensionalized by b/U_∞ and U_∞^2 respectively. All other nondimensional variables are unchanged. The linearized potential flow equations can now be easily formulated by again expanding the nondimensional pressure, density and acceleration potential in terms of ϵ . Substituting these

expansions into equation (8) yields

$$\bar{\phi}_0 + \epsilon \bar{\phi}_1 + O[\epsilon^2] = \int_0^{\bar{p}_1} \left[\frac{d\bar{p}_0}{\bar{\rho}_0} + \frac{d\bar{p}_1}{\bar{\rho}_1} \right] \left[1 - \epsilon \frac{\bar{p}_1}{\bar{p}_0} + O[\epsilon^2] \right] \quad (18)$$

Thus,

$$\bar{\phi}_0 = \text{constant, for } \bar{p}_0 = \text{constant; and } \bar{\phi}_1 = -\bar{p}_1/\bar{\rho}_0.$$

The linearized field equations can also be easily obtained. First, Eulers equation becomes

$$\frac{\partial \bar{u}_1}{\partial \bar{t}} = -\frac{1}{\bar{\rho}_0} \frac{\partial \bar{p}_1}{\partial \bar{x}} \quad \text{and} \quad \frac{\partial \bar{v}_1}{\partial \bar{t}} = -\frac{1}{\bar{\rho}_0} \frac{\partial \bar{p}_1}{\partial \bar{y}} \quad (19a,b)$$

where the convective acceleration terms are $O[\epsilon^2]$. Similarly, the continuity equation becomes

$$\bar{\rho}_0 \left(\frac{\partial \bar{u}}{\partial \bar{x}} + \frac{\partial \bar{v}}{\partial \bar{y}} \right) + \frac{\partial \bar{\rho}_1}{\partial \bar{t}} = 0 \quad (20)$$

Equations (19) and (20) can be combined to yield

$$\nabla^2 \bar{p}_1 - \frac{1}{a^2} \frac{\partial^2 \bar{p}_1}{\partial \bar{t}^2} = 0 \quad (21)$$

For an incompressible fluid the speed of sound, a , approaches infinity and the linearized equation becomes

$$\nabla^2 \bar{\phi}_1 = 0 \quad (22)$$

where the substitution $\bar{\phi}_1 = \bar{p}_1/\bar{\rho}_0$ was made in equation (22).

Finally, the acceleration components can be linearized as follows:

From equation (2) for two dimensional flow we obtain

$$\frac{\partial \bar{\phi}}{\partial \bar{X}} = \frac{D\bar{u}}{D\bar{t}} \quad \text{and} \quad \frac{\partial \phi}{\partial \bar{Y}} = \frac{D\bar{v}}{D\bar{t}} \quad (23a,b)$$

Substituting the asymptotic expansion for $\bar{\phi}$ and noting that $\bar{u} = \bar{u}_0 + \epsilon \bar{u}_1(\bar{X}, \bar{Y}, \bar{t}) + O(\epsilon^2)$, and equating equal powers of ϵ yields

$$\frac{\partial \bar{\phi}_1}{\partial \bar{X}} = \bar{u}_0 \frac{\partial \bar{u}_1}{\partial \bar{X}} + \frac{\partial \bar{u}_1}{\partial \bar{t}} \quad (24)$$

Similarly, for $\partial \phi_1 / \partial \bar{Y}$, we obtain

$$\frac{\partial \bar{\phi}_1}{\partial \bar{Y}} = \bar{u}_0 \frac{\partial \bar{v}_1}{\partial \bar{X}} + \frac{\partial \bar{v}_1}{\partial \bar{t}} \quad (25)$$

Having formulated the general linearized unsteady equations the solution for the potential flow region and the boundary layer will be discussed separately.

3.0 POTENTIAL FLOW SOLUTION

Within the framework of linearized theory, individual solutions may be superimposed to generate the complete solution. Thus, the flow field of an oscillating airfoil with "small" but finite thickness and camber can be obtained by the superposition of an unsteady airfoil of zero thickness and camber and a steady-state solution for an airfoil of small thickness and camber. However, in this analysis the characteristics of the two distinct unsteady effects, i.e., oscillating airfoil vs oscillating free stream, were of primary interest. For this reason, as a first approximation, it was decided to look at the steady state component for the airfoil with zero thickness and camber. This approximation permits closed form analytical solutions to the potential flow. This provides valuable physical insight into the role of the bound vorticity and the added mass effect. In addition, it provides a reference point for further investigations which can include both small but finite thickness and camber effects.

3.1 Thin Airfoil Solution

Under these restrictions, the equation describing the unsteady effects can be written below, where here and in subsequent equations the overbar for the nondimensional terms is dropped.

$$\frac{\partial^2 \phi}{\partial x^2} + \frac{\partial^2 \phi}{\partial y^2} = 0 \quad (26)$$

The steady state velocity is independent of x , and the linearized acceleration components are given by equations (24) and (25).

Referring to Figure 1, we can write the boundary conditions at the airfoil surface as

$$(v_1)_S = \frac{Dh}{Dt} = \frac{\partial h}{\partial t} + U_0 \frac{\partial h}{\partial X} \quad (27)$$

and

$$\left(\frac{\partial^2 \phi_1}{\partial Y^2} \right)_S = \frac{D^2 h}{Dt^2} = \frac{\partial^2 h}{\partial t^2} + 2U_0 \frac{\partial^2 h}{\partial X \partial t} + U_0^2 \frac{\partial^2 h}{\partial X^2} \quad (28)$$

where $h(X,t)$ describes the position of the airfoil. In addition to these conditions we require u_1 and $v_1 \rightarrow 0$ as $(X^2 + Y^2)^{1/2} \rightarrow \infty$, plus ϕ_1 must be finite at the trailing edge. This last condition is known as the Kutta-Joukowski condition. Unfortunately, due to the conformal transformation the acceleration potential will not be finite at the leading edge. This singularity and its subsequent elimination will be discussed in Section 3.2.

It is now that the powerful mathematical techniques of potential theory can be exploited. It is well known that a two dimensional airfoil can be treated by conformal mapping. Since the linearized boundary conditions are expanded about $-1 < X < 1$ and $Y = 0$, we can map this into a circle by

$$Z = \frac{1}{2} \left(Z^* + \frac{1}{Z^*} \right)$$

Thus the boundary conditions in the physical Z plane can be written in the conformal Z^* plane (see figure 4) as

$$\left(\frac{\partial \phi_1}{\partial n} \right)_S (r=1, \theta = \cos^{-1} X, t) = \left(\frac{\partial \phi_1}{\partial y} \right)_S (X, 0, t) \sin \theta \quad (29)$$

In addition, the condition at infinity can be written as

$$\lim_{|Z^*| \rightarrow \infty} \text{Real } \{w\} = \text{constant} \quad (30)$$

where w is the complex acceleration potential given by

$$w = \phi_1 + i\psi_1 = f(X + iY) \quad (31)$$

In the Z^* plane, w has the form

$$w(Z^*) = i \frac{A}{Z^* + 1} + i \frac{B}{Z^*} \quad (32)$$

where A and B are determined from the prescribed motion of the airfoil by applying the boundary and Kutta conditions.

3.1.1 Vertical Oscillation of Airfoil

For an airfoil undergoing vertical translation oscillations described by $h = a \cos \omega t$, the solution to the acceleration potential is given by

$$\frac{\phi_1}{\rho_0} = \{-ik C(k) \tan(\frac{\cos^{-1} X}{2}) + k^2 \sin(\cos^{-1} X)\} e^{i \frac{\alpha}{2} \tau} \quad (33)$$

where $X = 2\zeta - 1$ (see Figure 3), $K = \frac{\omega b}{U_\infty} = \frac{\alpha}{2}$ and $C(k) = F(k) + iG(k)$. The function $C(k)$ is known as Theodorsen's function and its value along with the details of the solution can be found in Ref. [9]. From the definition of ϕ_1 we see that the unsteady pressure gradient, which is of interest in the boundary layer analysis is simply

$$\frac{\partial p_1}{\partial \zeta} = 2 \frac{\partial}{\partial X} \left(\frac{\phi_1}{\rho_0} \right) \quad (34)$$

Performing the indicated differentiation, and after lengthy simplifications we obtain the unsteady pressure gradient in boundary layer coordinates given by

$$\frac{\partial p_1}{\partial \zeta} = \frac{1}{4\zeta^{2/3}(1-\zeta)^{1/2}} \{(\alpha G - \alpha^2(2\zeta-1)\zeta) - i\alpha F\} e^{i\tau} \quad (35)$$

The corresponding "edge" velocity can then be found from the unsteady Bernoulli equation in nondimensional boundary layer coordinates given by

Equation (9).

At this point, the potential analysis would be complete for the oscillating airfoil if it were not for the leading edge, i.e. $z \rightarrow 0$, singularity which is apparent from equation (35).

3.1.2 Vertical Oscillation of Free Stream

The second unsteady flow field in this investigation is that of a uniform flow in the X direction plus a small periodic component in the Y direction as shown in Figure 2b. With coordinates fixed on the airfoil, the effect of this oscillation in dimensional form can be expressed by $Y = h(X)e^{i\omega t}$. The boundary condition on the airfoil surface given by equation (26) becomes

$$(v_1)_S = \frac{\partial h}{\partial t} + U_0 \frac{\partial h}{\partial X} \quad (36)$$

In nondimensional form we have $Y = h(X) e^{i\frac{\alpha}{2}t}$, thus

$$(v_1)_S = (i\frac{\alpha}{2}h + \frac{dh}{dX})e^{i\frac{\alpha}{2}t} \quad (37)$$

The unsteady transverse velocity may contain a spatial nonuniformity due to the physical limitations of the wind tunnel. In fact it is difficult to create a uniform transverse oscillating flow at the wind tunnel centerline. Typical transverse spatial distributions are shown in Figures 6 and 7 and the physical characteristics are discussed in Section 4.3. For computational purposes, $h(X)$ is taken to be $\cos X$, which closely approximates the distribution shown in Figure 6 and represents one of the more nonuniform conditions. For this distribution, the "upwash" on the airfoil becomes

$$(v_1)_S = (i\frac{\alpha}{2}\cos X - \sin X)e^{i\frac{\alpha}{2}t} \quad (38)$$

Again, omitting the details which can be found in Ref. [8] or [9], we obtain

the unsteady pressure distribution given by

$$P_1 = (2a_0 \tan(\frac{\cos^{-1}X}{2}) + 4 \sum_{n=1}^{\infty} a_n \sin(n \cos^{-1}X)) e^{\frac{i\alpha}{2}\bar{t}} \quad (39)$$

where

$$a_0 = c(k)[P_0 + P_1] - P_1 \quad (40)$$

$$a_n = \frac{ik}{2n} P_{n-1} + P_n - \frac{ik}{2n} P_{n+1}, \quad n \geq 1 \quad (41)$$

The P_n coefficients are defined in terms of the "gust" velocity. Using the relation (see Figure 4) $\theta = \cos^{-1}X$, the coefficients are

$$P_0 = \frac{1}{\pi} \int_0^{\pi} v_1(\theta, t) d\theta \quad (42)$$

$$P_n = -\frac{1}{\pi} \int_0^{\pi} v_1(\theta, t) \cos(n\theta) d\theta, \quad n \geq 1 \quad (43)$$

From this, the unsteady pressure gradient in boundary layer coordinates (ζ, η, τ) becomes

$$\frac{\partial P_1}{\partial \zeta} = \frac{1}{2\zeta^{3/2}(1-\zeta)^{1/2}} \{a_0 - 4\zeta \sum_{n=1}^{\infty} a_n [n \cos(n \cos^{-1}(2\zeta-1))] \} e^{i\tau} \quad (44)$$

Equation (44) is the counterpart to equation (39) for an oscillating airfoil in a steady uniform flow. In fact equation (44) does reduce to equation (39) if $h(x) \rightarrow a$ which implies $(v_1)_S \rightarrow i\frac{\alpha}{2} e^{i\tau}$. Then $P_0 = -i\frac{\alpha}{2}$ and $P_n = 0$ for $n \geq 1$ which implies $a_0 = -i\frac{\alpha}{2} C(k)$ and $a_1 = \frac{\alpha}{2}$.

Since the pressure gradient given by equation (44) can represent either of the two distinct unsteady flows, it was used in the boundary condition part of the boundary layer code to calculate the edge velocity $U_e(\zeta, \tau)$. A ten point Gaussian quadrature scheme was used, and the first twenty coefficients were calculated. The truncation accuracy of the series including twenty coefficients insured overall relative accuracy of 10^{-8} which is more than sufficient for the analysis.

As expected, the unsteady pressure gradient due to a periodic transverse oscillation convected over a stationary airfoil contains a leading edge singularity. This mathematical singularity must be avoided or removed in some logical manner so that the boundary layer equations can be integrated. The method selected to accomplish this is discussed in the next section.

3.2 Leading Edge Solution

Due to the conformal mapping, the pressure gradient has a ζ^{-2} singularity at the leading edge and a $\zeta^{-1/2}$ singularity at the trailing edge. The trailing edge mathematical singularity is convergent, however, the ζ^{-2} is not. One obvious way of avoiding this difficulty, which is suggested in Ref. [7] is to simply start the integration at a small distance from the leading edge at, say 4% chord. Although this does not significantly effect the unsteady lift calculations, it does produce significant changes in the boundary layer calculations and hence the unsteady drag. For this reason, the following method was selected for starting the boundary layer calculations: It is well known that the leading edge region of a two-dimensional airfoil can be approximated by the stagnation flow around a right circular cylinder. Consequently, the flow field at the stagnation point of a cylinder oscillating with the same amplitude and frequency as the airfoil can be used as initial values for both U_e and dP/dx in the boundary layer calculations.

For a cylinder oscillating vertically in an inviscid uniform flow, the appropriate field equation in terms of the stream function is simply

$$\nabla^2 \psi = 0 \quad (45)$$

The appropriate boundary condition on the surface in (r, θ) coordinates is

$$v_r = -\frac{1}{r} \frac{\partial \psi}{\partial \theta} = \dot{y}_0 \sin \theta \quad (46)$$

where \dot{y}_0 represents its velocity with respect to (X,Y) as shown in Figure 5.

Following the solution first described by G. I. Taylor [7], the circumferential velocity at $r = R$ is given by

$$v_\theta(R, \theta) = -\dot{y}_0 \cos \theta - 2U_\infty \sin \theta \quad (47)$$

Letting $\dot{y}_0 = a \cos \omega t$, we can easily write the edge velocity, U_e , in boundary layer coordinates as

$$U_e(x, t) = 2U_\infty \sin \frac{x}{R} + a\omega \cos \frac{x}{R} \sin \omega t \quad (48)$$

At the stagnation point $\sin \frac{x}{R} + \frac{x}{R}$ and equation (48) becomes

$$U_e(\zeta, \tau) = 4m\zeta - i\frac{\alpha}{2}\epsilon e^{i\tau} \quad (49)$$

where Equation (49) is nondimensional and $m \equiv b/R$.

The unsteady pressure gradient can now be found from equation (9) by expanding both P and U_e in terms of ϵ , which yields

$$-\frac{\partial P_1}{\partial \zeta} = \alpha \frac{\partial U_1}{\partial \tau} + U_0 \frac{\partial U_1}{\partial \tau} + U_1 \frac{\partial U_0}{\partial \zeta} \quad (50)$$

Noting from equation (49) that $U_0 = 4m\zeta$ and $U_1 = i\frac{\alpha}{2}e^{i\tau}$ and substituting into equation (50) yields

$$-\frac{\partial P_1}{\partial \zeta} = \left(\frac{\alpha^2}{2} - i2\alpha m\right)e^{i\tau} \quad (51)$$

The potential flow field is now completely specified by the pressure gradients given by equations (35) and (44) plus the stagnation point pressure gradient given by equation (51). It is interesting to compare equation (35) in the limit as $\zeta \rightarrow 0$. Looking at the real part of $\partial P_1/\partial \zeta$

which represents the added mass effect, i.e. neglecting the bound vorticity component, we have

$$\lim_{z \rightarrow 0} \operatorname{Real} \left\{ \frac{dp_1}{dz} \right\} = - \frac{\alpha^2}{2} \quad (52)$$

This is precisely the real part for the cylinder given by equation (51).

This is to be expected, since the cylinder has no circulation and we see that the singularity in equation (35) is due to the bound vorticity component.

4.0 BOUNDARY LAYER RESULTS

4.1 Thin Airfoil Solution

The solution to the boundary layer outside the leading edge region through $O[\epsilon]$ is given by integrating equations (14) and (15) with the appropriate boundary conditions and using the results of Section 3.1. Equation (14) represents the steady flow contribution for an airfoil of zero thickness and hence zero pressure gradient. This equation can be rewritten in the usual form by introducing the Blasius similarity variables given by

$$\eta_B \equiv \frac{y}{(\nu x/U_\infty)^{1/2}} \quad \text{and} \quad \psi_B \equiv \frac{\psi(x,y)}{(\nu x U_\infty)^{1/2}} = \frac{f_B(\eta_B)}{(\nu x U_\infty)^{1/2}}$$

From these two relations, it follows that

$$\eta = \zeta^{1/2} \eta_B \quad \text{and} \quad \psi_0(\zeta, \eta) = \zeta^{1/2} f_B(\eta_B) \quad (53a,b)$$

Substituting equations (53a,b) into Equation (14) yields

$$f_B''' - \frac{1}{2} f_B f_B'' = 0 \quad (54.)$$

with boundary conditions given by

$$f_B(0) = f_B'(0) = 0 \quad (55a,b)$$

$$f_B'(\eta_B \rightarrow \infty) \rightarrow 1 \quad (55c)$$

The result, as expected, is the well known Blasius solution.

Turning now to the unsteady component and using $u_0 = \partial \psi_0 / \partial \eta$ and $v_0 = -\partial \psi_0 / \partial \zeta$, equation (15) can be written as

$$\begin{aligned} \alpha \frac{\partial^2 \psi_1}{\partial \eta \partial \tau} + u_0 \frac{\partial^2 \psi_1}{\partial \zeta \partial \eta} - v_{0,\eta} \frac{\partial \psi_1}{\partial \eta} + v_0 \frac{\partial^2 \psi_1}{\partial \eta^2} \\ - u_{0,\eta} \frac{\partial \psi_1}{\partial \zeta} - \frac{\partial^3 \psi_1}{\partial \eta^3} = - \frac{\partial p_1}{\partial \zeta} \end{aligned} \quad (56)$$

where

$$u_0 = f_B' \quad \text{and} \quad v_0 = \frac{1}{2\zeta} (\eta_B f_B' - f_B) \quad (57a,b)$$

From equations (57) we see that in addition to the singularity in the pressure gradient at $\zeta = 0$, the coefficients also contain singularities. This presents no additional difficulty, since at $\zeta = 0$ the corresponding stagnation point boundary layer equations along with the pressure gradient given by equation (51) are used to start the integration.

The temporal variation in equation (56) can be separated by the complex exponential time factor. This is due to the linearity of the equation which is a consequence of the small amplitude transverse oscillation. Representing the stream function and the pressure gradient in the complex plane as

$$\psi_1(\zeta, \eta, \tau) = \Psi_1(\zeta, \eta) e^{i\tau} \quad (58)$$

and

$$p_1(\zeta, \tau) = \hat{p}_1(\zeta) e^{i\tau} \quad (59)$$

and substituting these into equation (56) yields

$$i\alpha \frac{\partial \Psi_1}{\partial \eta} + u_0 \frac{\partial^2 \Psi_1}{\partial \zeta \partial \eta} - v_{0,\eta} \frac{\partial \Psi_1}{\partial \eta} + v_0 \frac{\partial^2 \Psi_1}{\partial \eta^2} - u_{0,\eta} \frac{\partial \Psi_1}{\partial \zeta} - \frac{\partial^3 \Psi_1}{\partial \eta^3} = - \frac{d\hat{p}_1}{d\zeta} \quad (60)$$

This equation could be integrated by a straightforward finite difference method, however a more flexible hybrid scheme is adopted. First, the stream function and the pressure gradient are decomposed into their real and imaginary parts, i.e., $\psi = \psi_r + i\psi_i$. Then, only the ζ -direction is finite differenced according to

$$\frac{\partial \psi_r}{\partial \zeta} = \frac{\psi_r^n - \psi_r^{n-1}}{\Delta \zeta} + O(\Delta \zeta) \quad (61)$$

Substituting these results into equation (60) yields the following two equations in n :

$$\begin{aligned} \{\psi_r'''' - v_0 \psi_r'' + (v_{0,n} - \frac{u_0}{\Delta \zeta}) \psi_r' + \frac{u_{0,n}}{\Delta \zeta} \psi_r \\ + \alpha \psi_i' - \frac{dp_r}{d\zeta}\}^n = - \{\frac{u_0}{\Delta \zeta} \psi_r' - \frac{u_{0,n}}{\Delta \zeta} \psi_r\}^{n-1} \end{aligned} \quad (62)$$

$$\begin{aligned} \{\psi_i'''' - v_0 \psi_i'' + (v_{0,n} - \frac{u_0}{\Delta \zeta}) \psi_i' + \frac{u_{0,n}}{\Delta \zeta} \psi_i \\ - \alpha \psi_r' - \frac{dp_i}{d\zeta}\}^n = \{\frac{u_0}{\Delta \zeta} \psi_i' - \frac{u_{0,n}}{\Delta \zeta} \psi_i\}^{n-1} \end{aligned} \quad (63)$$

with the following boundary conditions:

$$\psi_r' = \psi_r = 0 \quad \text{at} \quad \eta = 0 \quad (64a,b)$$

$$\psi_r' \rightarrow U_r(\zeta) \quad \text{as} \quad \eta \rightarrow \infty \quad (64c)$$

$$\psi_i' = \psi_i = 0 \quad \text{at} \quad \eta = 0 \quad (65a,b)$$

$$\psi_i' \rightarrow U_i(\zeta) \quad \text{as} \quad \eta \rightarrow \infty \quad (65c)$$

Equations (62) through (65) constitutes a well posed coupled boundary value problem. Its solution is obtained by using a general purpose spline collocation code. This particular integration scheme was selected because it is more versatile, accurate and stable than a full finite difference approach when solving parabolic equations. The accuracy is controlled by the step size, $\Delta\zeta$, since the spline collocation integration in the n direction is essentially exact (relative error tolerance on the function can be set at 10^{-7} without convergence difficulties). In addition, as $\Delta\zeta \rightarrow 0$ the finite difference characteristics approach the continuum characteristics which are normal to the ζ axis. A final justification for adopting this scheme over full finite difference methods lies in its ability to easily incorporate moving boundaries. Recall that in the present formulation, the boundary conditions are applied to the mean position, i.e. $Y = 0$, of the oscillating airfoil. However, it would be of interest in future investigations to study the effect of applying the boundary condition to the moving surface while holding all other parameters constant. This would then require only slight modifications to the boundary layer code whereas for full finite difference methods moving boundaries would introduce major complications.

Before discussing the results of the numerical solution of equations (62) through (65) the equations valid in the neighborhood of $\zeta = 0$ will be developed. The solution of these stagnation point equations will provide the starting profile for the boundary layer calculations.

4.2 Leading Edge Solution.

The flow field near the leading edge is described by equations (14) through (17) along with the potential flow results of Section 3.2. The same

procedure used in the previous section will be followed in obtaining solutions for both the steady and unsteady flows. For the steady flow, the edge velocity near $z = 0$ is given by $U_e = 2U_\infty x/R$. Equation (14) can be rewritten if we define the following nondimensional variables:

$$\eta_H \equiv \frac{y}{(\nu R/2U_\infty)^{1/2}}, \quad \zeta_H \equiv \frac{x}{R}, \quad \psi_H \equiv \frac{\psi}{(2R\nu U_\infty)^{1/2}} \quad (66)$$

The edge velocity suggests that ψ_H be written as $\bar{\psi}_H = \zeta_H f_H(\eta_H)$. Comparing equations (7) and (66) we see that

$$\eta_H = 2m^{1/2} \eta, \quad \zeta_H = 2m\zeta, \quad \psi_0(\zeta, \eta) = \bar{m}^{1/2} \zeta_H f_H \quad (67)$$

Substituting equations (67) into equation (15) yields

$$f_H''' + f_H f_H'' - f_H'^2 + 1 = 0 \quad (68)$$

with the following boundary conditions

$$f_H(0) = f_H'(0) = 0 \quad (69a,b)$$

$$f_H'(\eta_H \rightarrow \infty) \rightarrow 1 \quad (69c)$$

The solution as expected is the two dimensional Hiemenz stagnation point flow.

The corresponding unsteady equation can be obtained by first noting that

$$u_0 = \zeta f_H' \quad \text{and} \quad v_0 = -f_H \quad (70a,b)$$

Now writing $\bar{\psi}_1$, and \bar{p}_1 as $\psi_1 = \hat{\psi}_1(\eta)e^{i\tau}$ and $\hat{p}_1(\zeta)e^{i\tau}$ we obtain the $\hat{\psi}_1$ equation for the stagnation point region given by

$$i\alpha \frac{d\hat{\psi}_1}{d\eta} + 4mf'_H \frac{d\psi_1}{d\eta} - 2m^{1/2}f_H \frac{d^2\psi_1}{d\eta^2} - \frac{d^3\hat{\psi}_1}{d\eta^3} = -\frac{d\hat{p}_1}{d\zeta} \quad (71)$$

Notice that equation (71) is an ordinary differential equation whereas equation (60) is a partial differential equation. This is due to the fact that $U_1 = i \frac{\alpha}{2} e^{i\tau}$ which is independent of ζ . Equation (71) now represents a boundary value problem where the boundary conditions are

$$\hat{\psi}_1(0) = \hat{\psi}'_1(0) = 0 \quad (72a,b)$$

and

$$\hat{\psi}'_1(\eta \rightarrow \infty) \rightarrow -\frac{\alpha}{2} \quad (72c)$$

The solution is accomplished as before by using a general purpose spline collocation code to find $\hat{\psi}_1$. This is then used as the starting profile for the unsteady boundary layer solution. The details of the procedure can be found in the Appendix A.

4.3 Results and Discussion

As stated in the Introduction, the objective of this investigation is to compare the unsteady surface shear stress created on a thin airfoil undergoing transverse oscillations to that created by a transverse oscillating flow field. In both cases, a steady uniform flow approaches the airfoil from far upstream. Also, as discussed in the Introduction, the transverse oscillation is created by a wind tunnel with a time varying wall porosity. Thus, the actual spatial distribution of this velocity field

that the airfoil experiences will in general be a function of $L/H, M_\infty$, and the entrance length from the beginning of the porous section to the leading edge of the airfoil. Typical results of the spatial distribution calculated by incompressible potential theory are shown in Figure 6. The details of this solution are outlined in Appendix B. In this figure, the transverse velocity at the tunnel centerline is shown for various values of L/H , without any obstructions in the test section. It is obvious that the parameter L/H has a strong influence on the spatial distribution. For $L/H \rightarrow 1$ the distribution is approximately $\cos x$ whereas for $L/H \rightarrow \infty$ the spatial distribution becomes uniform.

Subsonic compressible flow distributions are shown in Figure 7 from Ref. [4] for purposes of comparison. In this case the Mach number is an additional parameter, and the two curves become identical as $M_\infty \rightarrow 0$ as expected.

Once the various parameters, i.e. L/H and the entrance length, are fixed the spatial and temporal transverse velocity at the tunnel centerline is taken as an input for the boundary layer calculations. Obviously, the presence of the airfoil will slightly alter this distribution, however in the present analysis, this "blockage" effect was neglected. It can be argued that this does not represent a serious limitation in the present analysis since other effects such as tunnel wall boundary layers, non uniformity of the tunnel wall porosity, three dimensional effects, and higher harmonics created by the actual oscillating flow would be ignored in a potential flow analysis which included the presence of the thin airfoil. In any case, the present boundary layer analysis would still be applicable since only the free stream pressure gradient and edge velocity would be altered and this is treated as simply a boundary condition in the present study.

As noted above, in the limit as L/H goes to infinity, the centerline transverse velocity becomes uniform and equal in magnitude to the wall velocity. For this condition the oscillating flow field yields the same unsteady pressure gradient and edge velocity (and hence the same shear stress behavior) as the oscillating airfoil except in the leading edge region. This discrepancy in the L.E. region is due to the mathematical artifice employed to remove the leading edge singularity and start the boundary layer calculations. Even with the discrepancy at the leading edge, the relative difference of integrated shear stress for the oscillating airfoil vs. uniform oscillating transverse flow is less than 1%. Consequently, only the effect of a nonuniform spatial distribution in the transverse velocity needs to be considered.

A spatial distribution given by $h(X) = \cos X$ was selected for comparison with the case of an airfoil oscillating in a uniform flow. This represents one of the worst possible conditions created by a zero entrance length, L_e , and L/H near unity. In both cases the frequency and amplitude are identical. Typical boundary layer velocity profiles for the two cases for various values of α are shown in Figures 8 and 9, at the 50% chord location. Notice that for the oscillating airfoil, the free stream disturbance velocity monotonically approaches zero as α approaches zero. This is apparent from the form of the pressure gradient given by equation (35) whereas for the oscillating free stream this is not true. Also notice as α approaches zero, the velocity profiles in Figure 9 contain very little "overshoot", i.e. the maximum value is approximately the same as the free stream value. This is to be expected since $\alpha \rightarrow 0$ implies a quasi-steady flow in the boundary layer. And, finally, notice that the unsteady boundary layer thickness is approximately equal to the Blasius boundary layer, i.e. $\eta \approx 5$. This is a conse-

quence of the scaling employed such that when $\alpha = 0[1]$, $\delta s/\delta_B = 0[1]$ at the mid chord location.

The results of most interest are shown in Figure 10. This represents the integrated non-dimensional wall shear stress as a function of the non-dimensional frequency, α , for both the oscillating airfoil and the oscillating free stream. As expected both curves go through the origin, since $\alpha = 0$ implies no oscillation. Notice that for large values of α , both curves asymptotically approach a constant value and the integrated shear stress for the oscillating airfoil is approximately 20% less than that for an oscillating free stream. However, this limit must be interpreted cautiously since α was restricted to be $0[1]$ in the perturbation analysis.

5.0 APPENDIXES

Appendix A

The system of equations given by (62) and (63) along with boundary conditions (64) and (65) represents a coupled set of third order boundary value problems. The solution of this set yields the first order unsteady disturbance for either an oscillating airfoil or a fixed airfoil with an oscillating transverse free stream. The difference between the two cases being the unsteady pressure gradient in (62) and (63) and the unsteady edge velocity in (64c) and (65c). For purposes of this discussion, the equations are written as

$$\psi_r''' = f_1(\eta, \psi_r, \psi_r', \psi_r'', \psi_i') \quad (\text{A.1})$$

$$\psi_i''' = f_2(\eta, \psi_i, \psi_i', \psi_i'', \psi_r) \quad (\text{A.2})$$

This set of equations is solved by the use of a general purpose boundary value code known as COLSYS. This code uses the method of spline-collocation at Gaussian points and is described in detail in reference [10]. Only the main "driver" for this code along with the details for obtaining the local inviscid unsteady pressure gradient is discussed in this section.

The four subroutines unique to the COLSYS code are: FSUB, DFSUB, GSUB, and DGSUB. FSUB is the subroutine for evaluating f_1 and f_2 at each η in the interval $0 \leq \eta \leq \eta_\infty$. DFSUB is the subroutine for evaluating the Jacobian of f_1 and f_2 at each η . And similarly, GSUB and DGSUB determine the appropriate boundary conditions and the Jacobian respectively.

The subroutine A determines the a_n coefficients in equation (44) which are given by (40) and (41). And, finally, the subroutine BC determines the edge velocities U_r and U_i by solving the perturbation form of equation (9), which is

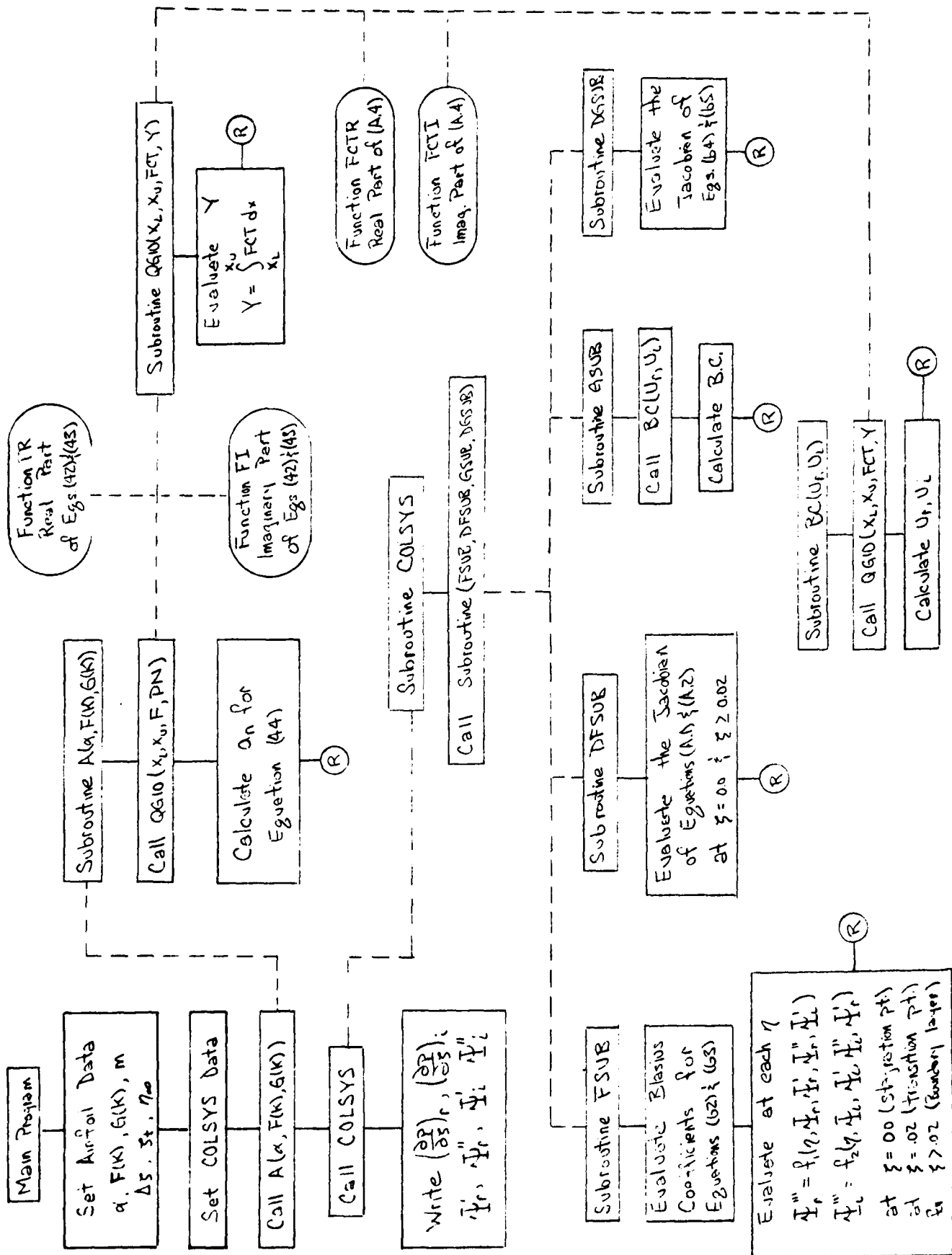
$$-\frac{\partial \bar{p}_1}{\partial \zeta} = \alpha \frac{\partial \bar{U}_1}{\partial \tau} + \frac{\partial \bar{U}_1}{\partial \zeta} \quad (\text{A.3})$$

Separating out the periodic component, i.e. $e^{i\tau}$, (A.3) can be written in integral form as

$$\bar{U}_1 = -e^{-i\alpha\zeta} \int_0^\zeta \frac{dp}{d\zeta} e^{i\alpha\zeta} d\zeta \quad (\text{A.4})$$

This equation is then integrated using the Gaussian quadrature subroutine QG10.

A highly schematized diagram of this procedure plus a listing of the driver program is given next.



```

IMPLICIT REAL*8(A-H,O-Z)
COMMON/A1/SF1R,SF2R,SF1I,SF2I,XS,ZT,DPDZR,DPDZI
COMMON/A2/DLZ,78
COMMON/A4/ALPHA,GK,FK,C
COMMON/A6/AR,AT
REAL*8 ZETA(6),ESPACE(40000),TOL(4),Z(6),SF1R(41),SF2R(41),SF3R(41-
1),SF1I(41),SF2I(41),SF3I(41),AR(21),AT(21)
INTEGER ISPACF(2500),M(2),IPAR(11),LTOL(4)
EXTERNAL FSUB,DFSUB,GSUB,DGSUB,FCTH,FCTI,FR,FI

```

C
C

```

NCOMP=2
M(1)=3
M(2)=3

```

C

```

ALPHA=1.2
FK=.5788
GK=-.1378
CALL A(ALPHA,FK,GK)
DO 5 I=1,21
5 WRITE(6,8)I,AR(I),AT(I)
8 FORMAT(1X,I4,2F14.6)
XS=20.0
DLZ=.0200
C=5.
ZT=.03
NS=50

```

C
C

```

ALFFT=0.000
ARIGHT=XS
ZETA(1)=0.000
ZETA(2)=0.000
ZETA(3)=0.000
ZETA(4)=0.000
ZETA(5)=XS
ZETA(6)=XS

```

C
C

```

IPAR(1)=0
IPAR(2)=0
IPAR(3)=0
IPAR(4)=4
IPAR(5)=40000
IPAR(6)=2500
IPAR(7)=1
DO 10 K=8,11
10 IPAR(K)=0

```

C

```

DO 20 L=1,4
LTOL(L)=L
20 TOL(L)=0.1D-3

```

C

```

C
  ZS=0.000
  WRITE(6,30)ALPHA,ARIGHT
30  FORMAT(1H1,'ALPHA=',F7.3,4X,'FREE STREAM=',F10.4/)
  SSR=0.0
  SSI=0.0
  DO 200 IS=1,NS
  WRITE(6,40)ZS
40  FORMAT(///' ZS = ',F7.3//)
  CALL COLSYS(NCOMP,N,ALEFT,ARIGHT,ZETA,IPAR,ITOL,TOL,FXPAT,ISPACE,
  1 FSPACE,IFLAG,FSUB,DFSUB,GSUB,OGSUB,SOLUTN)
  WRITE(6,45)DPDZR,DPDZI
45  FORMAT(' DPDZR = ',F10.3,' DPDZI = ',F10.3/)
  X=0.000

```

```

C
  DO 100 IC=1,41
  CALL APPSLN(X,Z,FSPACE,ISPACE)
  SF1R(IC)=Z(1)
  SF2R(IC)=Z(2)
  SF3R(IC)=Z(3)
  SF1I(IC)=Z(4)
  SF2I(IC)=Z(5)
  SF3I(IC)=Z(6)
  X=X+.025*XS
100 CONTINUE

```

```

C
  X=0.0
  DO 110 IP=1,11
  WRITE(6,120)X,SF2R(IP),SF3R(IP),SF2I(IP),SF3I(IP)
  X=X+.025*XS
110 CONTINUE
120 FORMAT(6X,F5.2,4X,4D15.5)
  X=X+.025*XS
  DO 130 IP=13,41,2
  WRITE(6,120)X,SF2R(IP),SF3R(IP),SF2I(IP),SF3I(IP)
  X=X+.05*XS
130 CONTINUE
  SSR=SSR+SF3R(1)
  SSI=SSI+SF3I(1)
  ZS=ZS+DLZ
200 CONTINUE
  WRITE(6,300)SSR,SSI
300 FORMAT(1X,'TOTAL SHEAR STRESS =',2F14.4)
  STOP
  END

```

```

SUBROUTINE FSUB(X,Z,F)
IMPLICIT REAL*8(A-H,O-Z)
COMMON/A1/SF1R,SF2R,SF1I,SF2I,X1,Z1,DPL78,DPD71
COMMON/A2/DLZ,ZS
COMMON/A3/UO,OUN,VU,VUM
COMMON/A4/ALPHA,GK,FK,C
COMMON/A5/DPR0,DPR1,DPR2,DP10,DP11,DP12
COMMON/A6/AR,AI
DIMENSION Z(6),F(2),SF1R(41),SF2R(41),SF1I(41),SF2I(41)
DIMENSION AR(21),AI(21)

```

```

C
IF(ZS.EQ.0.0001)GO TO 120
XB = X/DSQRT(ZS)

```

```

C
IL=1
IR=2
DLX=.02500**XS
XL=0.000
XR=XL+DLX
5 IF(XR.GE.YL.AND.X.LT.XR)GO TO 10
XL=XL+DLX
XR=XR+DLX
IL=IL+1
IR=IR+1
GO TO 5
10 SF1RX=SF1R(IL)+(SF1R(IR)-SF1R(IL))*(X-XL)/(XR-XL)
SF2RX=SF2R(IL)+(SF2R(IR)-SF2R(IL))*(X-XL)/(XR-XL)
SF1IX=SF1I(IL)+(SF1I(IR)-SF1I(IL))*(X-XL)/(XR-XL)
SF2IX=SF2I(IL)+(SF2I(IR)-SF2I(IL))*(X-XL)/(XR-XL)

```

```

C
IF(XR-5.0)40,40,50
40 F0=.008225**XB+.0146794**XB**2+.016132**XB**3+.006004**XB**4+.000041
19**XB**5
F0=.008225**XB+.0146794**XB**2+.016132**XB**3+.006004**XB**4+.000041
19**XB**5
F0P=.008225**XB+.0146794**XB**2+.016132**XB**3+.006004**XB**4+.000041
19**XB**5
F0P=.008225**XB+.0146794**XB**2+.016132**XB**3+.006004**XB**4+.000041
19**XB**5
GO TO 60
50 F0=5.28320+(XR-5.0)
F0P=1.0
F0P=0.0
60 UO=F0P/ZS**0.5
VO=1.0/2.0/73**0.5*(XB*F0-F0)
VOP=0.5/73**XB*F0P

```

```

C
IF(ZS.EQ..0200)GO TO 300
TMR=UO*SF2RX/DL7-UOP*SF1RX/DL7
TMI=UO*SF2IX/DL7-UOP*SF1IX/DL7
ZC=1.0/(2.0*ZS**1.5*DSQRT(1.0-7.0))
DPDZ=70*AR(1)

```

```

SUBROUTINE FSUB(X,Z,F)
IMPLICIT REAL*8(A-H,O-Z)
COMMON/A1/SF1R,SF2R,SF1I,SF2I,X1,Z1,DPLZS,DPRZ1
COMMON/A2/DLZ,ZS
COMMON/A3/U0,U0R,V0,V0R
COMMON/A4/ALPHA,GK,FK,C
COMMON/A5/DPR0,DPR1,DPR2,DPI0,DPI1,DPI2
COMMON/A6/AR,AI
DIMENSION Z(6),F(2),SF1R(41),SF2R(41),SF1I(41),SF2I(41)
DIMENSION AR(21),AI(21)

```

```

IF(ZS.EQ.0.0001)GO TO 120
XR = X/DSQRT(7S)

```

```

IL=1
IR=2
DLX=.02500*XS
XL=0.000
XR=XL+DLX
5 IF(XR.GE.YL.AND.X.LT.YR)GO TO 10
XL=XL+DLX
XR=XR+DLX
IL=IL+1
IR=IR+1
GO TO 5

```

```

10 SF1RX=SF1R(IL)+(SF1R(IR)-SF1R(IL))*(X-XL)/(XR-XL)
SF2RX=SF2R(IL)+(SF2R(IR)-SF2R(IL))*(X-XL)/(XR-XL)
SF1IX=SF1I(IL)+(SF1I(IR)-SF1I(IL))*(Y-XL)/(YR-XL)
SF2IX=SF2I(IL)+(SF2I(IR)-SF2I(IL))*(X-XL)/(XR-XL)

```

```

IF(XR-5.0)40,40,50
40 F0=.008225*XB+.0146799*XB**2+.016132*XB**3+.006004*XB**4+.0.00041...
19*XB**5
F0P=.0324177*XF+.015439*XB**2+.009181*XB**3+.000859*XB**4+.0.0002...
1142*XB**5
F0PP=.033206+.016247*XB+.036485*XB**2+.037509*XB**3+.0.008560*XB**...
1*XB**4+.0.0008388*XB**5
GO TO 60
50 F0=5.28320+(XR-5.0)
F0P=1.0
F0PP=0.0
60 U0=FP
U0R=F0P/ZS**0.5
V0=1.0/2.0/7S**0.5*(XR*FP-F0)
V0R=0.5/7S*XB*F0P

```

```

IF(ZS.EQ..02001)GO TO 300
INRR=U0*SF2RX/DLZ-U0R*SF1RX/DLZ
INRI=U0*SF2IX/DLZ-U0R*SF1IX/DLZ
ZC=1.0/(2.0*ZS**1.5*DSQRT(1.0-7S))
DPRZ=7C*AR(1)

```

```

DPDZ1=ZC*AI(1)
DO 70 M=2,10
XM=M-1
AZ=XM*0.408(2.0*78-1.0)
SC=4.0*78*XM*0.408(AZ)
DPDZR=DPDZR-SC*7C*AR(M)
70 DPDZI=DPDZI-SC*7C*AI(M)
DPR2=DPDZR
DPI2=DPDZI

```

```

C
40 F(1)=V0*Z(3)-(V0N-U0/DLZ)*Z(2)-U0N*Z(1)/DLZ+ALPHA*Z(5)+DPDZR-TNHR
F(2)=V0*Z(6)-(V0N-U0/DLZ)*Z(5)-U0N*Z(4)/DLZ+ALPHA*Z(2)+DPDZI-TNHI
RETURN

```

```

C
C
120 XR=2.*X*DSQRT(C)
IF(XR-2.0) 200,200,210
200 F0=-.00107*XR + .52432*XR**3 - .16657*XR**3. + .02249*XR**4.
FP=1.24*XR - .53*XR*XR + .064*XR**3.
GO TO 220
210 F0=1.3624 + .995*(XR-2.0)
FP=1.0
220 V0=-2.0*F0*DSQRT(C)
V0N=-4.0*FP*C
DPDZR=-ALPHA*ALPHA/2.0
DPDZI=2.0*ALPHA*C
DPR0=DPDZR
DPI0=DPDZI

```

```

C
F(1)=V0*Z(3)-V0N*Z(2)-ALPHA*Z(5)+DPDZR
F(2)=V0*Z(6)-V0N*Z(5)+ALPHA*Z(2)+DPDZI
RETURN

```

```

C
C
300 ZC=1.0/(2.0*ZT**1.5*DSQRT(1.0-ZT))
DPDZR=ZC*AR(1)
DPDZI=ZC*AI(1)
DO 310 M=2,10
XM=M-1
AZ=XM*0.408(2.0*7T-1.0)
SC=4.0*7T*XM*0.408(AZ)
DPDZR=DPDZR-SC*7C*AR(M)
310 DPDZI=DPDZI-SC*7C*AI(M)
DPDZI=(DPDZI+DPI0)/2.0
DPDZR=(DPDZR+DPR0)/2.0
DPR1=DPDZR
DPI1=DPDZI
TNHR=U0*SF2RX/DLZ-U0N*SF1RX/DLZ
TNHI=U0*SF2IX/DLZ-U0N*SF1IX/DLZ

```

```

C
F(1)=V0*Z(3)-(V0N-U0/DLZ)*Z(2)-U0N*Z(1)/DLZ+ALPHA*Z(5)+DPDZR-TNHR
F(2)=V0*Z(6)-(V0N-U0/DLZ)*Z(5)-U0N*Z(4)/DLZ+ALPHA*Z(2)+DPDZI-TNHI
RETURN
END

```

```

SUBROUTINE DFCUB(X,Z,DF)
IMPLICIT REAL*8(A-H,O-Z)
COMMON/A2/DLZ,ZS
COMMON/A3/U0,U0N,V0,V0N
COMMON/A4/ALPHA,GK,FK,C
DIMENSION DF(2,6),Z(6)

```

C

```

IF(ZS.F0.0.0)GO TO 20
DF(1,1)=-U0N/DLZ
DF(1,2)=-V0N+U0/DLZ
DF(1,3)=V0
DF(1,4)=0.000
DF(1,5)=-ALPHA
DF(1,6)=0.000
DF(2,1)=0.000
DF(2,2)=ALPHA
DF(2,3)=0.000
DF(2,4)=-U0N/DLZ
DF(2,5)=-V0N+U0/DLZ
DF(2,6)=V0
RETURN

```

C

```

20 DF(1,1)=0.000
DF(1,2)=-V0N
DF(1,3)=V0
DF(1,4)=0.00
DF(1,5)=-ALPHA
DF(1,6)=0.000
DF(2,1)=0.000
DF(2,2)=ALPHA
DF(2,3)=0.000
DF(2,4)=0.000
DF(2,5)=-V0N
DF(2,6)=V0
RETURN
END

```

```

SUBROUTINE FSUB(I,Z,G)
IMPLICIT REAL*8(A-H,O-Z)
DIMENSION Z(6)

```

C

```

GO TO (1,2,3,4,5,6),I
1 G=Z(1)
RETURN
2 G=Z(2)
RETURN
3 G=Z(4)
RETURN
4 G=Z(5)
RETURN
5 CALL AC(UR,UI)
G=Z(2)-UR
RETURN
6 CALL BC(UR,UI)
G=Z(5)-UI
RETURN
END

```

```

      SUBROUTINE DGSUB(I,Z,DG)
      IMPLICIT REAL*8(A-H,O-Z)
      DIMENSION Z(6),DG(6)
      DO 10 J = 1,6
10  DG(J) = 0.000
      GO TO (1,2,3,4,5,6),I
      1  DG(1)=1.000
      RETURN
      2  DG(2)=1.000
      RETURN
      3  DG(4)=1.000
      RETURN
      4  DG(5)=1.000
      RETURN
      5  DG(2)=1.000
      RETURN
      6  DG(5)=1.000
      RETURN
      END

```

```

      SUBROUTINE A(ALPHA,FK,GK)
      IMPLICIT REAL*8(A-H,O-Z)
      DIMENSION AR(21),AI(21),PR(22),PI(22)
      COMMON/A6/AR,AI
      COMMON/A7/K1
      EXTERNAL FR,FI
      DO 50 N=1,22
      K1=N
      XL=0.0
      XU=3.1415927
      CALL QG10(XL,XU,FR,PNR)
      CALL QG10(XL,XU,FI,PNT)
      PR(N)=-PNR/3.1415927
50  PI(N)=-PNT/3.1415927
      AR(1)=FK*(PR(1)+PR(2))-PR(2) - GK*(PI(1)+PI(2))
      AI(1)=GK*(PR(1)+PR(2)) + FK*(PI(1)+PI(2))-PI(2)
      DO 60 N=2,21
      AR(N)=-1.25*ALPHA/(N-1))*(PI(N-1)-PI(N+1))+PR(N)
60  AI(N)=-(.25*ALPHA/(N-1))*(PR(N-1)-PR(N+1))+PI(N)
      RETURN
      END

```

```

SUBROUTINE RC(UR,UI)
IMPLICIT REAL*8(A-H,O-Z)
COMMON/A2/DLZ,ZS
COMMON/A4/ALPHA,GK,FK,C
COMMON/A5/DPR0,DPR1,DPR2,DPI0,DPI1,DPI2
EXTERNAL FCTR,FCTI

```

```

C
IF(ZS.LE.0.0500)GO TO 10
C
XL=0.04
XU=ZS
CALL OG10(XL,XU,FCTR,YR)
CALL OG10(XL,XU,FCTI,YI)
UR =-YR*DCOS(ALPHA*ZS)- YI*DSIN(ALPHA*ZS) + UR2
UI = YR*DSIN(ALPHA*ZS)- YI*DCOS(ALPHA*ZS) + UI2
RETURN
C
10 IF(ZS=0.0200)40,30,20
20 UR=UR1-DLZ*(DPR1+DPR2)/2.0
UI=UI1-DLZ*(DPI1+DPI2)/2.0
UR2=UR
UI2=UI
RETURN
30 UP=UR0-DLZ*(DPR0+DPR1)/2.0
UI=UI0-DLZ*(DPI0+DPI1)/2.0
UR1=UR
UI1=UI
RETURN
40 UR=0.0
UI=-ALPHA/2.0
UR0=UP
UI0=UI
RETURN
END

```

```

SUBROUTINE OG10(XL,XU,FCT,Y)
IMPLICIT REAL*8(A-H,O-Z)
EXTERNAL FCTR,FCTI,FR,FI
A=0.5*(XU+XL)
B=XU-XL
C=0.4869533*B
Y=0.6333567*(FCT(A+C)+FCT(A-C))
C=0.4325317*B
Y=Y+.07472567*(FCT(A+C)+FCT(A-C))
C=0.3497048*B
Y=Y+.1095432*(FCT(A+C)+FCT(A-C))
C=0.2166972*B
Y=Y+.1346334*(FCT(A+C)+FCT(A-C))
C=0.07443717*B
Y=B*(Y+.1477621*(FCT(A+C)+FCT(A-C)))
RETURN
END

```

```

FUNCTION FT(THETA)
IMPLICIT REAL*8(A-H,O-Z)
COMMON/A4/ALPHA,GK,FK,C
COMMON/A7/K1
VI=ALPHA/2.0
FI=VI*DCOS((K1-1)*THETA)
RETURN
END

```

```

FUNCTION FR(THETA)
IMPLICIT REAL*8(A-H,O-Z)
COMMON/A7/K1
VR=0.0
FR=VR*DCOS((K1-1)*THETA)
RETURN
END

```

```

FUNCTION FCTI(ZS)
IMPLICIT REAL*8(A-H,O-Z)
DIMENSION AR(21),AI(21)
COMMON/A4/ALPHA,GK,FK,C
COMMON/A6/AR,AI
ZC=1.0/(2.0*ZS**1.5*DSQRT(1.0-ZS))
FCTI=DSIN(ALPHA*ZS)*ZC*AR(1)+DCOS(ALPHA*ZS)*ZC*AI(1)
DO 100 M=2,10
XM=M-1
AZ=XM*DARCOS(2.0*ZS-1.0)
SC=4.0*ZS*XM*DCOS(AZ)
100 FCTI=FCTI-DSIN(ALPHA*ZS)*ZC*SC*AR(M)-DCOS(ALPHA*ZS)*ZC*SC*AI(M)
RETURN
END

```

```

FUNCTION FCIR(ZS)
IMPLICIT REAL*8(A-H,O-Z)
DIMENSION AR(21),AI(21)
COMMON/A4/ALPHA,GK,FK,C
COMMON/A6/AR,AI
ZC=1.0/(2.0*ZS**1.5*DSQRT(1.0-ZS))
FCIR=DCOS(ALPHA*ZS)*ZC*AR(1)-DSIN(ALPHA*ZS)*ZC*AI(1)
DO 100 M=2,10
XM=M-1
AZ=XM*DARCOS(2.0*ZS-1.0)
SC=4.0*ZS*XM*DCOS(AZ)
100 FCIR=FCIR-DCOS(ALPHA*ZS)*ZC*SC*AR(M)+DSIN(ALPHA*ZS)*ZC*SC*AI(M)
RETURN
END

```

Appendix B

The actual flow field induced by temporal variations of the test section wall porosity to an otherwise incompressible uniform wind tunnel flow is a function of the Reynolds number, entrance length (L_e), L/H , and the geometry of the model in the test section. Other effects such as free stream turbulence, the details of the flow through the porous section and the frequency of oscillation can be important. However, a reasonable approximation to the unsteady oscillations can be obtained in analytical form if a potential flow model is adopted. This is the same basic restriction employed in reference [4].

Referring to Figure 11, and considering the effect of the variable wall porosity without any obstructions in the test section, the potential function is given by solving

$$\nabla^2 \phi = 0 \quad (B.1)$$

subject to the following boundary conditions

$$\left. \frac{\partial \phi}{\partial y} \right|_{y=0,H} = \begin{cases} V_0(x) \cos \omega t & , \quad -\frac{L}{2} \leq x \leq \frac{L}{2} \\ 0 & , \quad |x| \geq \frac{L}{2} \end{cases} \quad (B.2)$$

$$\frac{\partial \phi}{\partial x} \rightarrow U_\infty \quad \text{and} \quad \frac{\partial \phi}{\partial y} \rightarrow 0 \quad \text{as} \quad |x| \rightarrow \infty \quad (B.3)$$

The solution to this system of equations can be found in closed form by using the Fourier Transform Method. First writing $\phi(x,y,t) = \phi_s(x,y) \cos \omega t$, as a consequence of linearity of the system, and then introducing the Fourier

transform defined below.

$$\phi(s, y) = \frac{1}{\sqrt{2\pi}} \int_{-\infty}^{+\infty} \phi_s(x, y) e^{-isx} dx \quad (B.4)$$

The original system of equations becomes

$$\frac{d^2 \phi}{dy^2} - s^2 \phi = 0, \quad (B.5)$$

with the boundary condition

$$\left. \frac{d\phi}{dy} \right|_{y=0, H} = V_0(s), \quad (B.6)$$

where

$$V_0(s) = \frac{1}{\sqrt{2\pi}} \int_{-\infty}^{+\infty} V_0(x) e^{-isx} dx. \quad (B.7)$$

Solving for $d\phi/dy$, which is the variable of interest, we obtain

$$\frac{d\phi}{dy} = V_0(s) \frac{\sinh sy + \sinh s(H-y)}{\sinh sH}. \quad (B.8)$$

Taking the inverse transform and using (B.7) yields

$$\frac{\partial \phi}{\partial y} = \frac{1}{2\pi} \int_{-1/2}^{+1/2} V_0(\xi) \left\{ \int_{-\infty}^{+\infty} \frac{\sinh sy + \sinh s(H-y)}{\sinh sH} e^{is(x-\xi)} ds \right\} d\xi \quad (B.9)$$

Integrating (B.9) with respect to the transform variable s , yields

$$\begin{aligned}
\frac{\partial \phi_s}{\partial y} = & \frac{\sin \frac{\pi(H-y)}{2H}}{2H} \int_{-L/2}^{+L/2} \frac{V_0(\xi) d\xi}{\cosh \frac{\pi(x-\xi)}{H} + \cos \frac{\pi(H-y)}{H}} \\
& + \frac{\sin \frac{\pi y}{2H}}{2H} \int_{-L/2}^{+L/2} \frac{V_0(\xi) d\xi}{\cosh \frac{\pi(x-\xi)}{H} + \cos \frac{\pi y}{H}}
\end{aligned} \quad (B.10)$$

This is as far as the solution can be taken for arbitrary values of $V_0(\xi)$. However, for the uniform porosity situation, i.e. $V_0 = \text{constant}$, the solution can be found in closed form.

The final form, although lengthy, has certain advantages over a numerical solution and is given below, for $|x| \leq L/2$

$$\begin{aligned}
\frac{\partial \phi_s}{\partial y} = & \frac{V_0}{2\pi} \left\{ \sin^{-1} \frac{1+A^-}{B^+} + \sin^{-1} \frac{1+A^+}{C^+} \right. \\
& \left. + \sin^{-1} \frac{1-A^-}{B^-} + \sin^{-1} \frac{1-A^+}{C^-} \right\} - V_0
\end{aligned} \quad (B.11)$$

where

$$A^\pm = \cos \frac{\pi y}{H} \cosh \frac{\pi}{H} \left(x \pm \frac{L}{2} \right)$$

$$B^\pm = \cosh \frac{\pi}{H} \left(x - \frac{L}{2} \right) \pm \cos \frac{\pi y}{H}$$

$$C^\pm = \cosh \frac{\pi}{H} \left(x + \frac{L}{2} \right) \pm \cos \frac{\pi y}{H}$$

Similarly, for the region $|x| \leq \frac{L}{2}$, the y-component of velocity is given by

$$\frac{\partial \phi_s}{\partial y} = \frac{V_0}{2\pi} \left\{ \sin^{-1} \frac{1+A^-}{B^+} - \sin^{-1} \frac{1+A^+}{C^+} \right. \\ \left. + \sin^{-1} \frac{1-A^-}{B^-} - \sin^{-1} \frac{1-A^+}{C^-} \right\} \quad (B.12)$$

The results for various values of L/H are shown in Figure 6.

6.0 REFERENCES

1. McCroskey, W. J. "Some Current Research in Unsteady Fluid Dynamics/ The 1976 Freeman Scholar Lecture". ASME Transactions, Ser. 1, Journal of Fluids Engineering, Vol. 99, pp 8-39, March 1977.
2. Nishimura, H. and Matsushita, H. "Gus Response Experiments of an Airplane Dynamic Model in the NAL Gust Wind Tunnel". Transactions of the Japan Society for Aeronautical and Space Sciences, Vol. 20, No. 49, pp 138-150, October 1977.
3. Gilman, Jean, Jr. and Bennett, R. M., "A Wind-Tunnel Technique for Measuring Frequency Response Functions for Gust Load Analyses". AIAA Paper No. 65-787, November 1965.
4. Jacocks, J. L., et al., Evaluation of a New Concept for the Generation of Unsteady Flow in a Transonic Wind Tunnel, AEDC-TR-79-8, 1979.
5. Ostrach, S. "Compressible Laminar Boundary Layer and Heat Transfer for Unsteady Motions of a Flat Plate". NACA TN 3569, 1955.
6. Glauert, M. B., "The Laminar Boundary Layer on Oscillating Plates and Cylinders". J. Fluid Mech., Vol. 1, pp 97-110, 1956.
7. Taylor, G. I., "Motion of Solids in Fluids When the Flow is Irrotational", Proc. Roy Soc., A93 (1917) pp 99-113.
8. Bisplinghoff, R. L., Ashley, A., and Helfman, R. L., Aeroelasticity, Addison-Wesley, (1955).
9. Fung, Y. C., An Introduction to the theory of Aeroelasticity, Dover, pp 214, (1969).
10. Ascher, U., et al., "Collocation Software for Boundary Value ODE'S", Codes for Boundary Value Problems in Ordinary Differential Equations, Springer-Verlag, Berlin, pp 164-185, (1979).

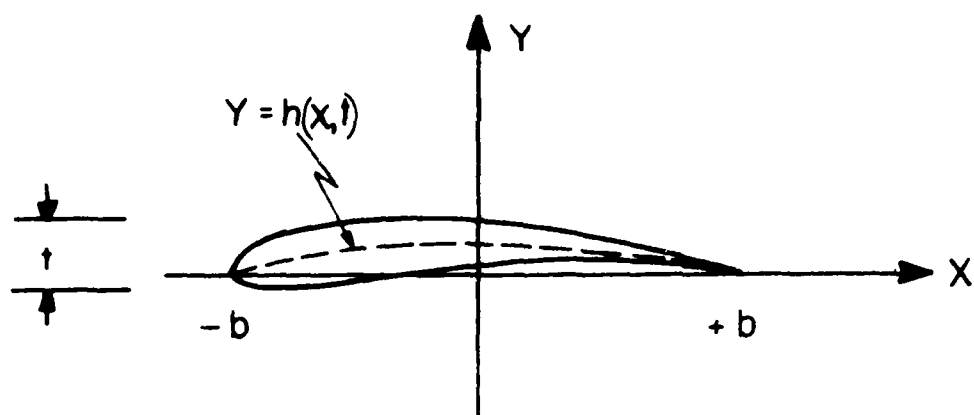


Figure 1. Airfoil geometry and coordinate system



Figure 2.a. Oscillating airfoil in a uniform stream

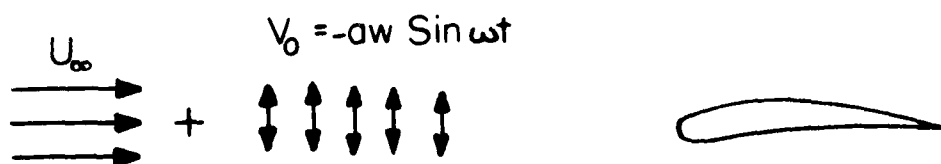


Figure 2.b. Fixed airfoil with an oscillating transverse flow

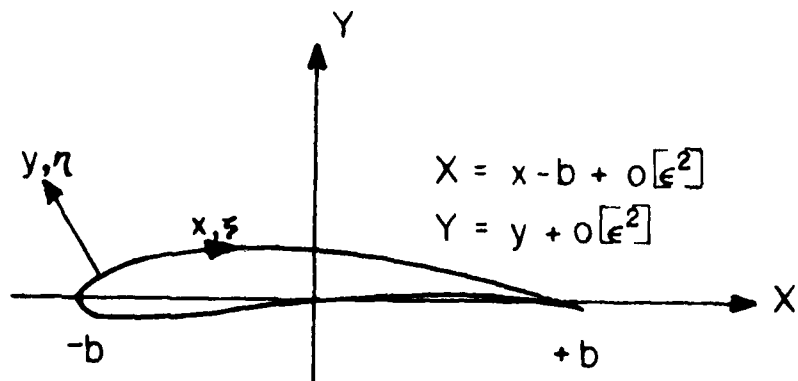


Figure 3. Potential flow and boundary layer coordinates

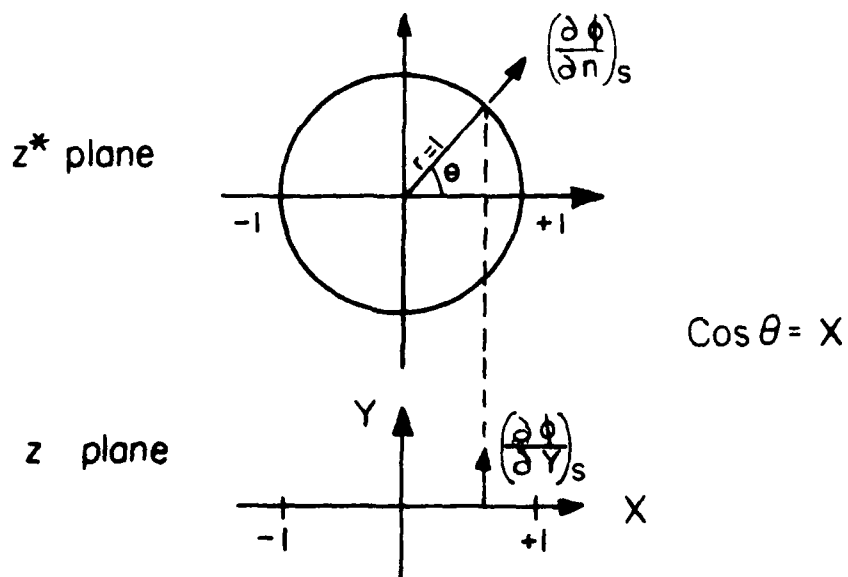


Figure 4. Conformal mapping of line segment into a circle

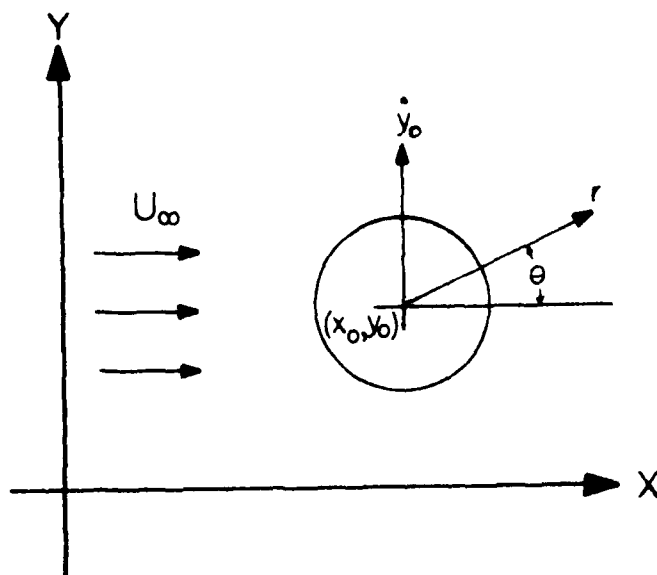


Figure 5. Circular cylinder oscillating in a uniform flow

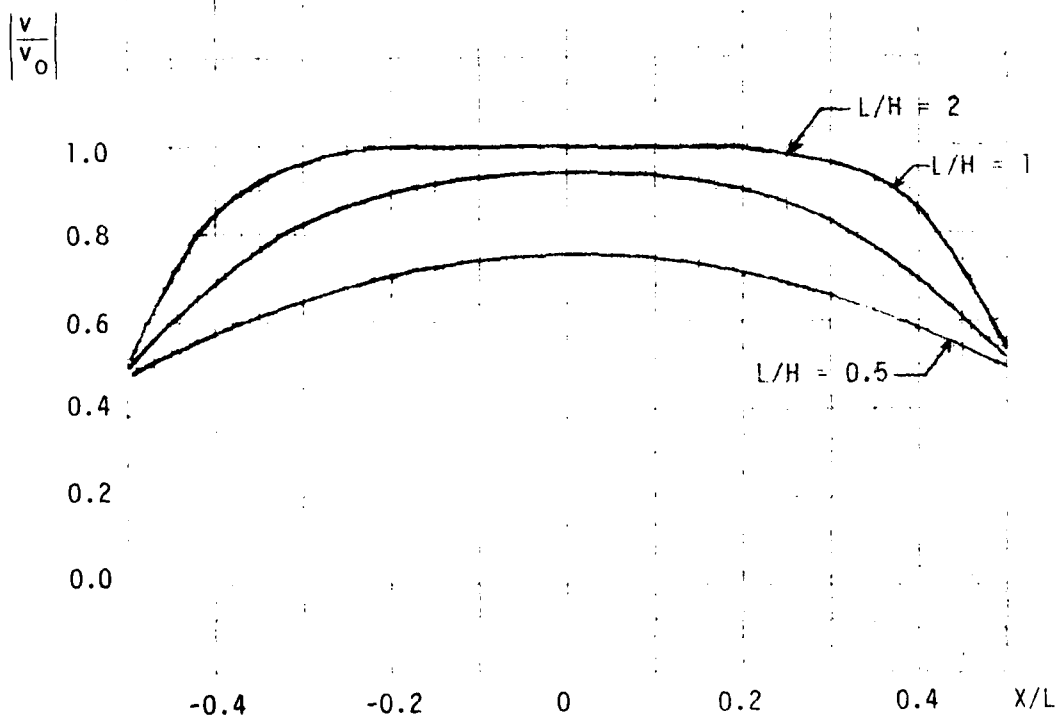
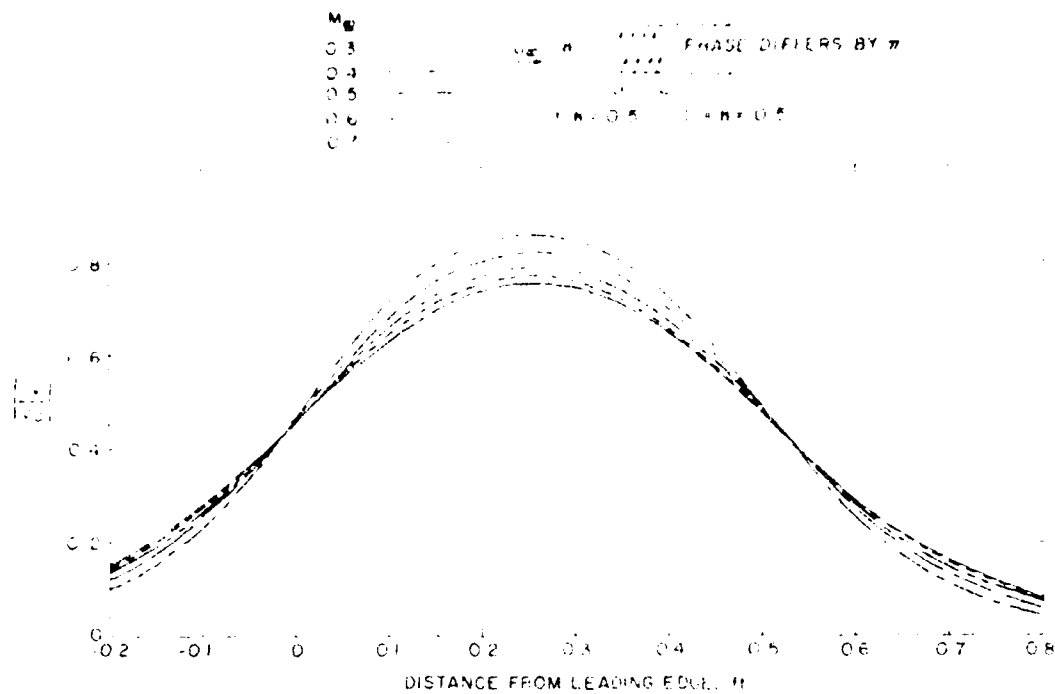
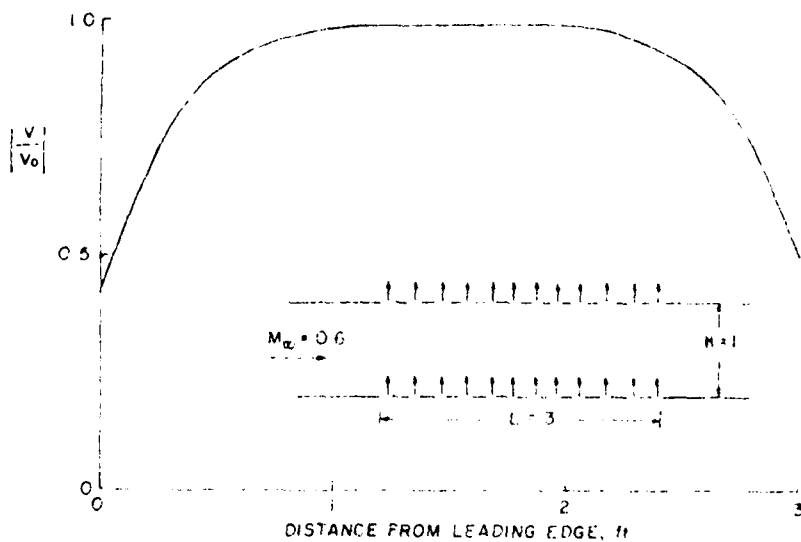


Figure 6. Spatial distribution of transverse velocity at wind tunnel centerline



Longitudinal distribution of flow angle amplitude for a symmetric ball-wall installation, $L/H = 1.0$.



Longitudinal distribution of flow angle amplitude for a symmetric ball-wall installation, $L/H = 3.0$.

Figure 7. Spatial distribution for subsonic compressible flow from reference [4]

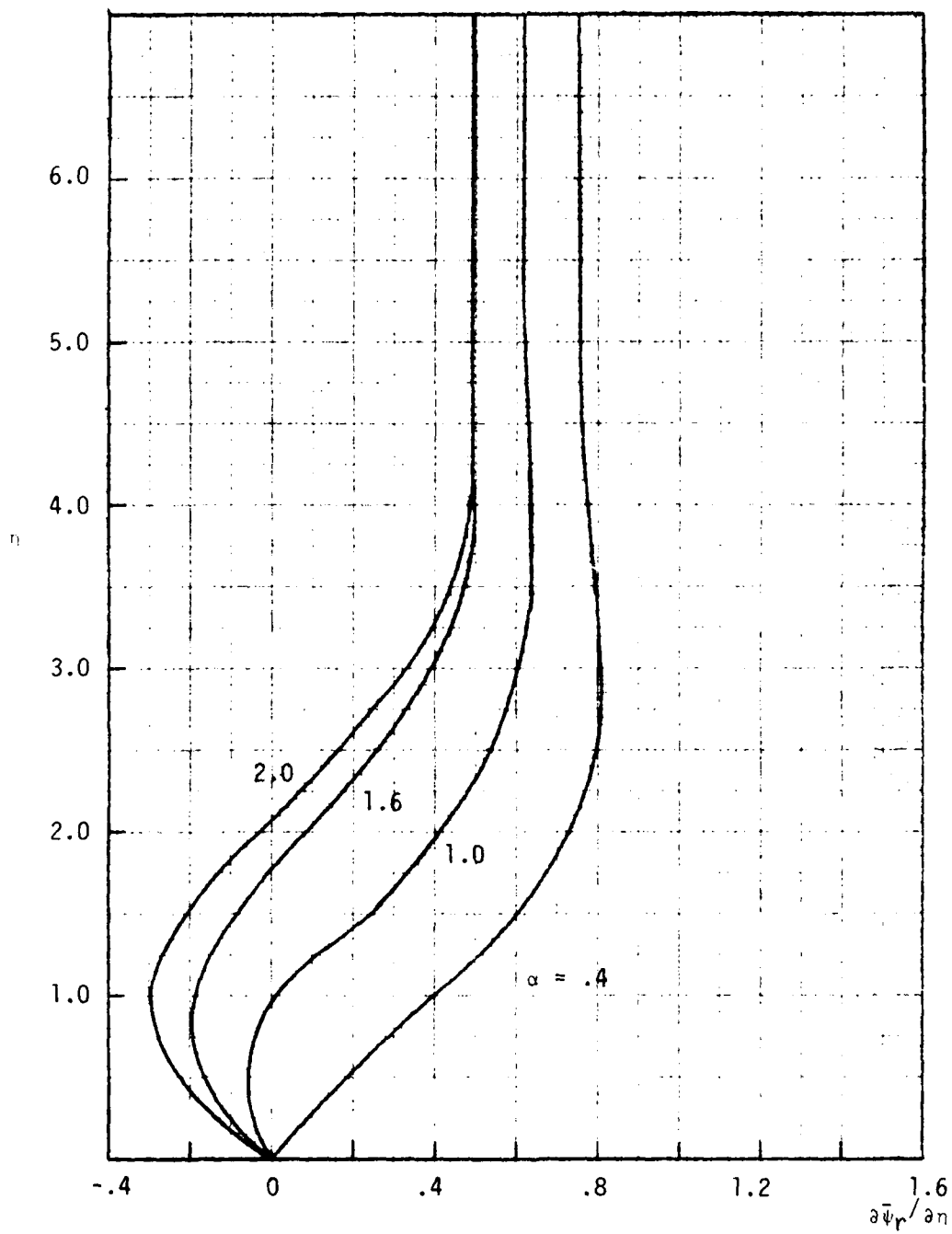


Figure 8a. Real part of the complex velocity for the oscillating free stream at $\zeta = 0.5$

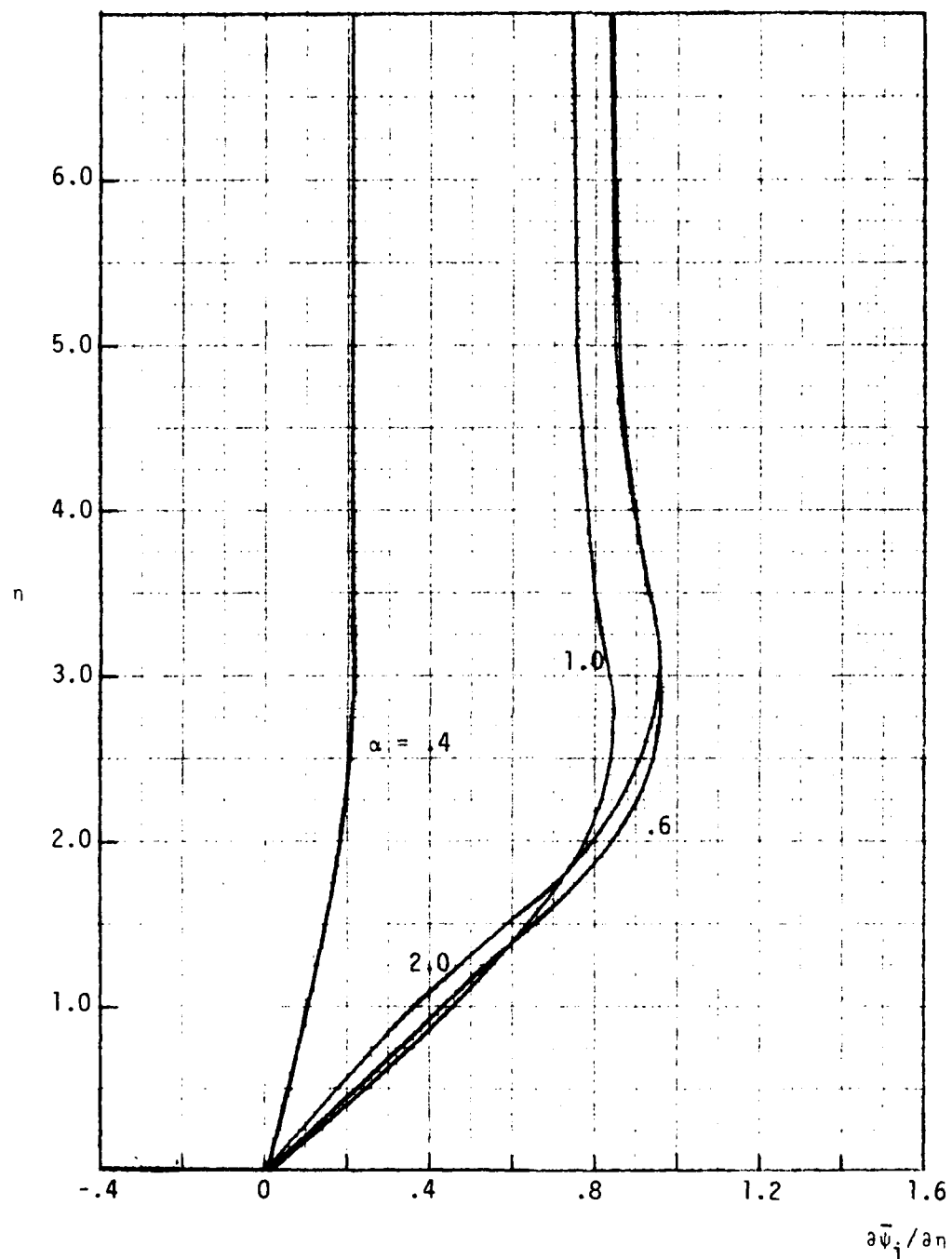


Figure 8b. Imaginary part of the complex velocity for the oscillating freestream at $\zeta = 0.5$

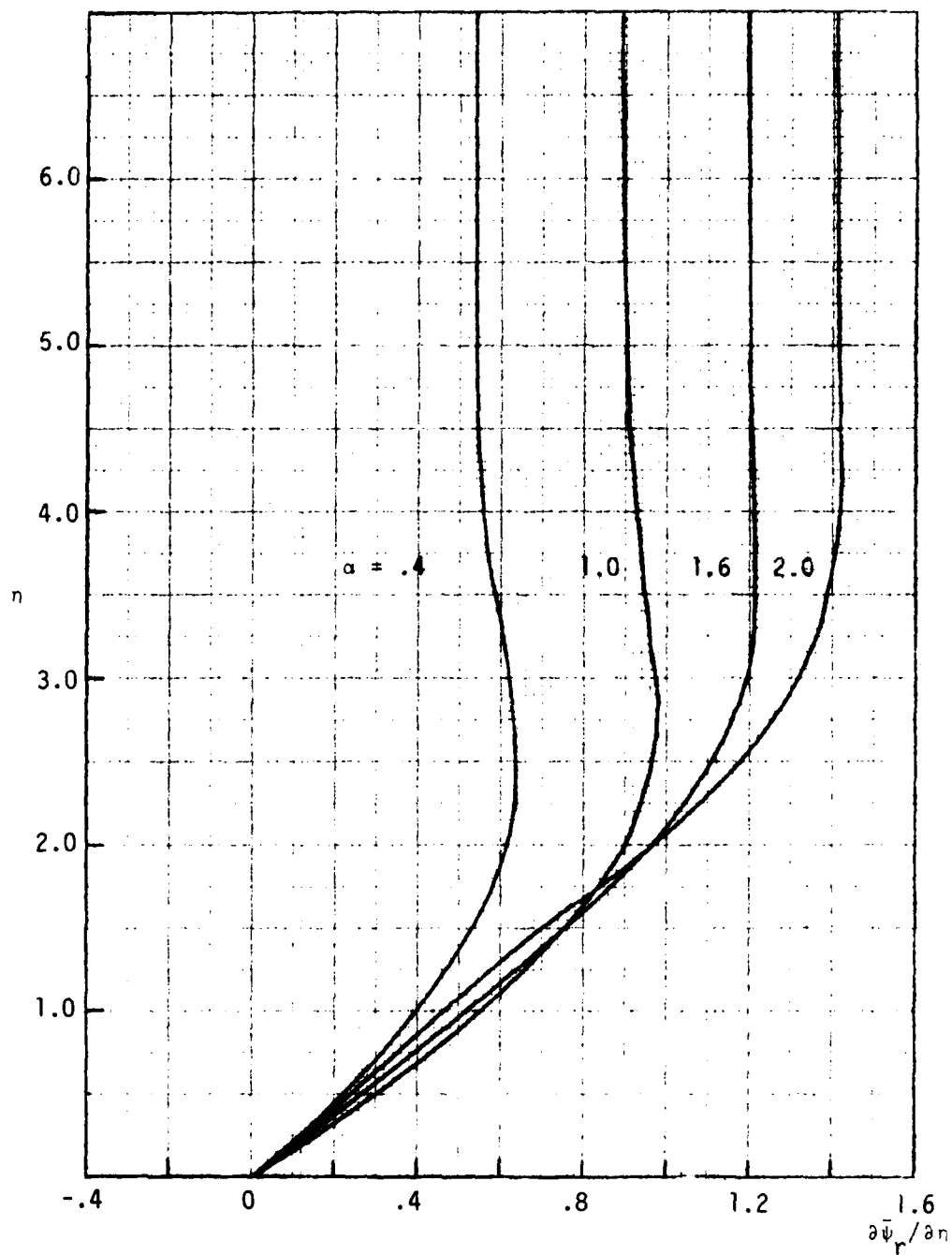


Figure 9a. Real part of the complex velocity for the oscillating airfoil at $\zeta = 0.5$

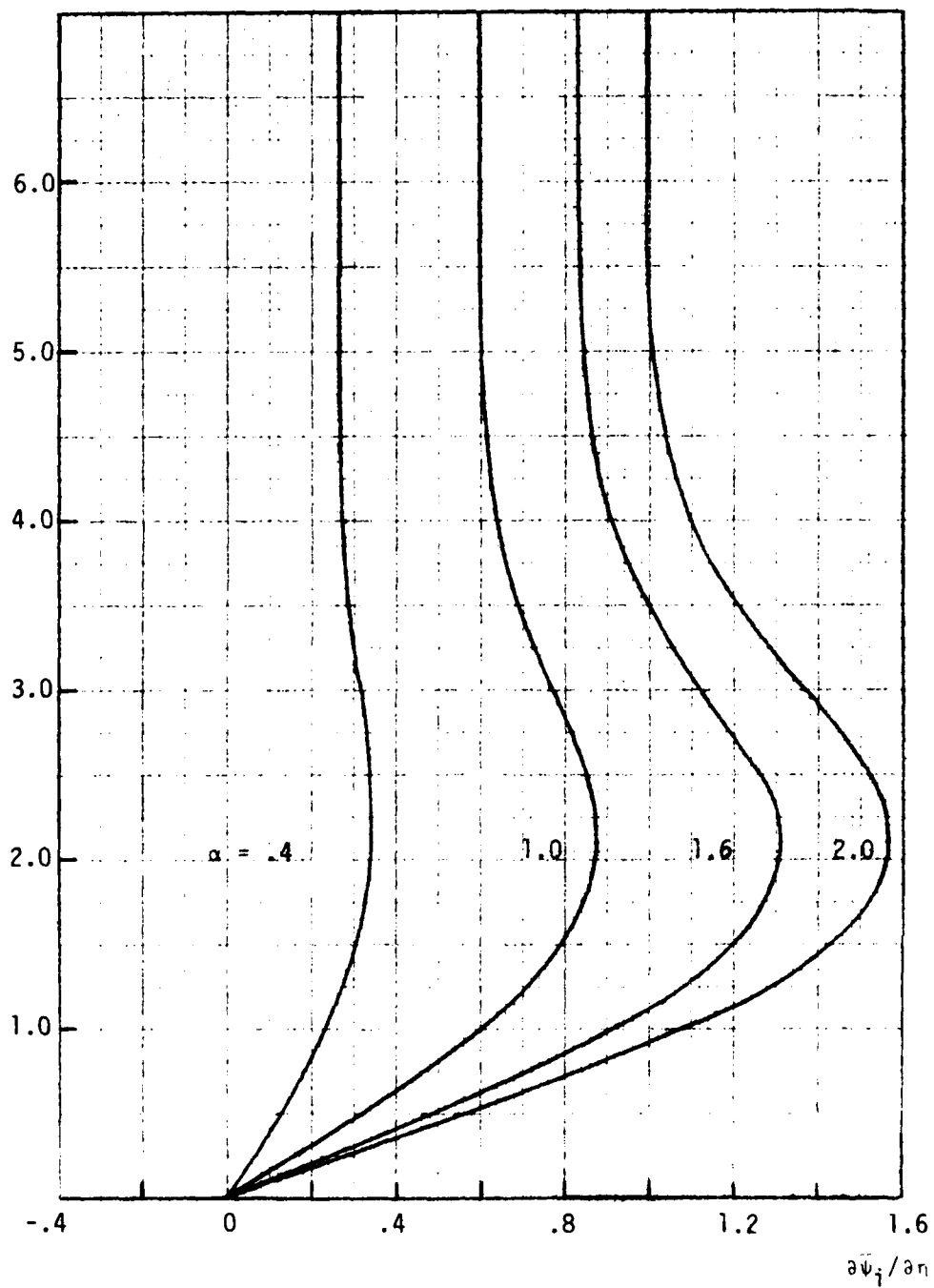


Figure 9b. Imaginary part of the complex velocity for the oscillating airfoil at $\zeta = 0.5$

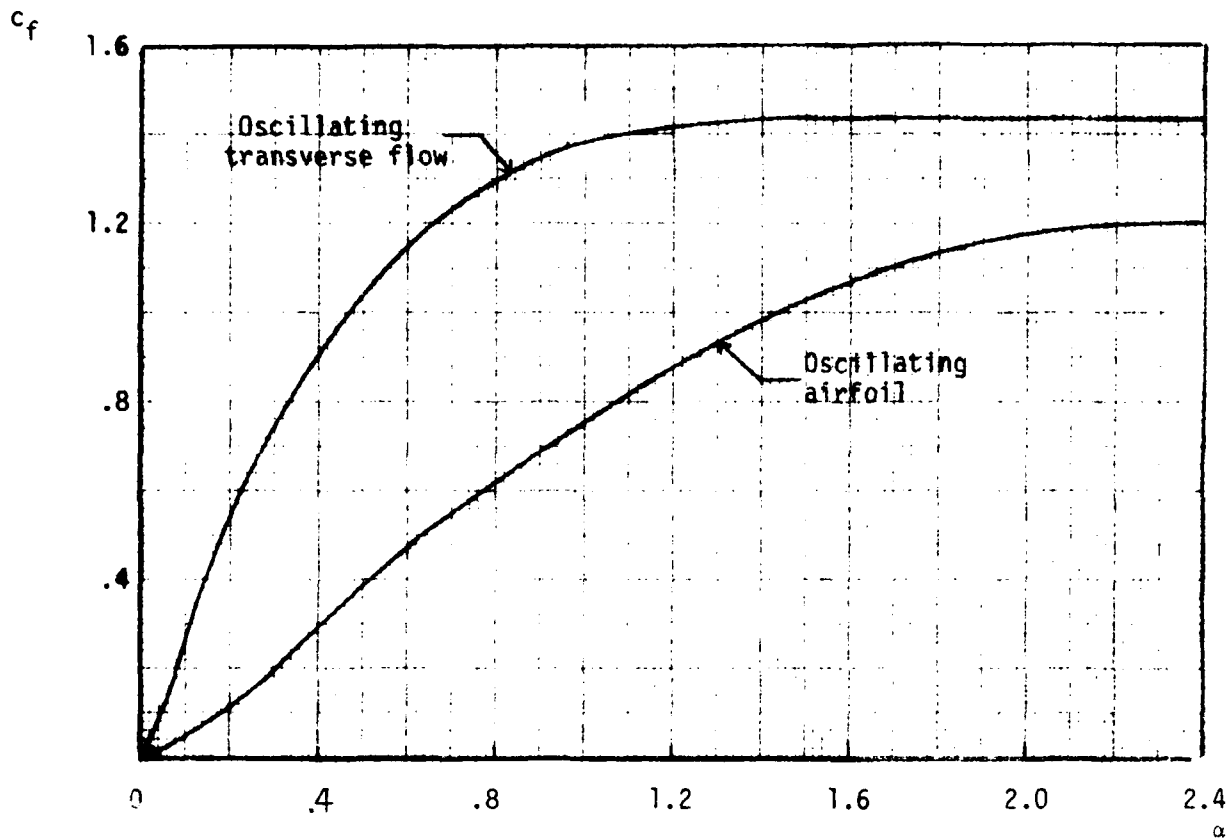


Figure 10. Nondimensional integrated shear stress vs. nondimensional frequency

$$c_f = \int_{-1}^{+1} \frac{\tau_w}{\rho U_\infty^2} Re^{1/2} d\tau$$

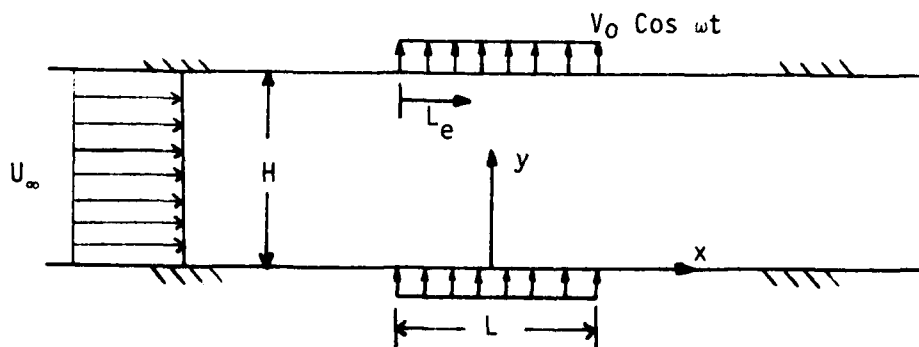


Figure 11. Geometry and notation for the potential flow solution